

1                   **Synthetic simulation of spatially-correlated**  
2                   **streamflows: Weighted-modified Fractional Gaussian**  
3                   **Noise**

4                   **Cristián Chadwick<sup>1</sup>, Frederic Babonneau<sup>2,3</sup>, Tito Homem-de-Mello<sup>4</sup>, Agustín**  
5                   **Letelier<sup>1</sup>**

6                   <sup>1</sup>Faculty of Engineering and Sciences, Universidad Adolfo Ibáñez, Diagonal Las Torres 2640, Peñalolén,  
7                   Santiago, Chile

8                   <sup>2</sup>Kedge Business School, 680 Cr de la Libération, 33405 Talence, France

9                   <sup>3</sup>ORDEC SYS, 4 Place de l'Etrier, CH-1224 Chêne-Bougeries, Suisse

10                  <sup>4</sup>School of Business, Universidad Adolfo Ibáñez, Diagonal Las Torres 2640, Peñalolén, Santiago, Chile

11                 **Key Points:**

- 12                 • We propose a Weighted modified Fractional Gaussian Noise (WmFGN) model that  
13                 addresses both temporal and spatial correlations simultaneously.
- 14                 • The method searches for an optimal convex combination of the spatial and tem-  
15                 poral correlation matrices according on the user's priority.
- 16                 • Our results on a Chilean basin demonstrate that WmFGN represents a significant  
17                 improvement over existing methods in preserving correlations.

---

Corresponding author: Cristián Chadwick, [cristian.chadwick@uai.cl](mailto:cristian.chadwick@uai.cl)

18 **Abstract**

19 Stochastic methods have been typically used for the design and operations of hy-  
 20draulic infrastructure. They allow decision makers to evaluate existing or new infrastruc-  
 21ture under different possible scenarios, giving them the flexibility and tools needed in  
 22 decision making. In this paper, we present a novel stochastic streamflow simulation ap-  
 23 proach able to replicate both temporal and spatial dependencies from the original data  
 24 in a multi-site basin context. The proposed model is a multi-site extension of the mod-  
 25 ified Fractional Gaussian Noise (mFGN) model which is well-known to be efficient to main-  
 26 tain periodic correlation for several time lags, but presents shortcomings in preserving  
 27 the spatial correlation. Our method, called Weighted-mFGN (WmFGN), incorporates  
 28 spatial dependency into streamflows simulated with mFGN by relying on the Cholesky  
 29 decomposition of the spatial correlation matrix of the historical streamflow records. As  
 30 the order in which the decomposition steps are performed (temporal then spatial, or vice-  
 31 versa) affects the performance in terms of preserving the temporal and spatial correla-  
 32 tion, our method searches for an optimal convex combination of the resulting correla-  
 33 tion matrices. The result is a Pareto-curve that indicates the optimal weights of the con-  
 34 vex combination depending on the importance given by the user to spatial and tempo-  
 35 ral correlations. The model is applied to Bio-bio River basin (Chile), where the results  
 36 show that the WmFGN maintains the qualities of the single-site mFGN, while signif-  
 37 icantly improving spatial correlation.

38 **1 Introduction**

39 Stochastic methods have been typically used to improve and evaluate the design  
 40 and operation of existing or new hydraulic infrastructures, e.g., the evaluation of reser-  
 41 voir performance using stochastic streamflows by Hashimoto et al. (1982). Stochastic stream-  
 42 flow generation allows the evaluation of infrastructure, under different scenarios, of us-  
 43 age, public policies, operation, and even under climate change conditions (Kirsch et al.,  
 44 2013). Due to the new challenges that water resources are facing, such as climate change,  
 45 as well as changes in public policies in the changing world, robust stochastic methods  
 46 able to simulate synthetic streamflows consistent with historical records, capable of in-  
 47 corporating possible changes are required.

48        Multiple synthetic streamflow generation models have been developed in the lit-  
49        erature, to answer both to scientific and decision maker needs of scenarios evaluation.  
50        These stochastic generation models work at a single or multi-site scale to replicate the  
51        statistical behaviour of streamflows. The advantage of multi-site models is that they can  
52        evaluate scenarios over an entire basin at the same time. There have been several dis-  
53        cussions in literature to determine the most complete stochastic multi-site streamflow  
54        model, without getting to consensus (Srinivas & Srinivasan, 2005). To the best of our  
55        knowledge, methods always fail for simulating muti-site streamflows on at least one di-  
56        mension, e.g., temporal correlation, capture of seasonality, spatial correlation, or long-  
57        run dependencies. In this paper, we present a novel stochastic streamflow simulation ap-  
58        proach able to replicate both temporal and spatial dependencies from the original data  
59        in a multi-site basin context.

60        Initial studies in stochastic hydrology were based on booststrap techniques (Efron  
61        & Tibshirani, 1994), generating time-series from the random sampling with replacement  
62        of historical records that lost any autocorrelation specific to the original series. This strat-  
63        egy was followed by several variants such as the method of moving blocks Bootstrap (Vogel  
64        & Shallcross, 1996; Srinivas & Srinivasan, 2005) and nearest neighbor Bootstrap (Lall  
65        & Sharma, 1996). The former method only partially corrects the autocorrelation issues,  
66        and the latter depends on the availability of historical data, which is a drawback if one  
67        wants to simulate stochastic change conditions as projected in (IPCC, 2021). In paral-  
68        lel to Bootstrap methods, the family of autoregressive (AR) models arose as a first or-  
69        der Markovian model (Thomas Harold, 1962). These methods later evolved with mul-  
70        tiple related works (Matalas, 1967; Moreau & Pyatt, 1970; Jettmar & Young, 1975; Young  
71        & Jettmar, 1976) to formalize the  $p$ -order AR ( $AR(p)$ ) models (Box et al., 2015), and  
72        the autoregressive moving average model (ARMA). Autorregressive models adequately  
73        incorporate autocorrelation in the time-series, but they assume that the autocorrelation  
74        is constant in time. This is an important limitation for the simulation of shorter time  
75        step streamflows (e.g. less than one year), as autocorrelation does change over the year,  
76        due to seasonality. In view of the above, periodic autoregressive models ( $PAR(p)$ ) have  
77        been proposed (Pagano, 1978; Parzen & Pagano, 1979; Salas et al., 1982), which are  $AR(p)$   
78        models using sets of autocorrelations specific to each time period (e.g., weekly or monthly).  
79        However, even when the  $PAR(p)$  manages to circumvent the  $AR(p)$  models autocorre-

80 lation problem, doubts arise as to how long the period should be (e.g. monthly or sea-  
81 sonally), or which parameter estimation methodology should be used (Noakes et al., 1985).

82 More recently, Copula-based autorregresive models have been proposed for multi-  
83 site runoff synthetic generation (Chen et al., 2015; Lee & Salas, 2011; Hao & Singh, 2013;  
84 de Almeida Pereira & Veiga, 2019; Pereira et al., 2017; Reddy & Ganguli, 2012). A ma-  
85 jor strength of the Copula-based models is their flexibility given that they adjust the cop-  
86 ulas to historical input data by using marginal distribution functions. These functions  
87 allow to simulate streamflows with scarce available information, showing great sensitiv-  
88 ity in the identification of nonlinear dependencies in the sampling, maintaining the struc-  
89 tural benefits and limitations of the PAR( $p$ ) or ARMA models. A monthly copulas model  
90 has been proposed in Xu et al. (2022) for flow forecasting that is highly capable of pre-  
91 dicting future short and medium-term flows in non-stationary contexts. Note that flow  
92 forecasting is used for decision making, but some strategic decisions require long-term  
93 simulations, which are not addressed by flow forecasting methods.

94 Attempts to integrate both temporal and spatial correlations for synthetic runoff  
95 generation have been proposed with trivariate copulas by Chen et al. (2015), which sim-  
96 ulates first a single streamflow (Lee & Salas, 2011), and then adds the multi-site corre-  
97 lation. Trivariate copulas are able to preserve cross-correlation between different trib-  
98 utaries at lag 0, and consistently replicate historical characteristics of the different sites  
99 such as mean, variance and autocorrelations in lags 1 and 2 (with larger but acceptable  
100 differences in the latter). However, similarly to Hao and Singh (2013), the marginal prop-  
101 erties of the copula cannot be directly estimated from data. They must be numerically  
102 approximated, which is a drawback in the use of the models as stated in (de Almeida Pereira  
103 & Veiga, 2019). Another application was developed by Pereira et al. (2017) through a  
104 two-stage model in which simulations for different sites (39 hydropower plants) are gen-  
105 erated independently with a PAR( $p$ ) model. The spatial correlations are then incorpo-  
106 rated in a second stage by means of vine-copulas as proposed in (Erhardt et al., 2015).  
107 In (de Almeida Pereira & Veiga, 2019), the authors developed a multi-site flow simula-  
108 tor based on copula autoregressive (COPAR) model previously used in economics (Brechmann  
109 & Czado, 2015). The COPAR model has a periodic component and directly solve the  
110 temporal and spatial relationships of the different tributaries with a multi-dimensional  
111 copula. As in Chen et al. (2015), it ensures spatial correlations in the simulations close  
112 to the historical ones up to lag 2, and mean autocorrelations consistent with the histor-

113       ical ones up to lag 5 (except for some months). The Copulas and other autoregressive  
 114       based models have the drawback of not being sensitive enough to replicate high histor-  
 115       ical temporal correlation (Kirsch et al., 2013).

116       Other methodologies used in hydrology that deal with the simulation of temporal  
 117       and spatial features simultaneously are introduced by Tsoukalas et al. (2018a, 2018b).  
 118       These authors design a new family of Nataf-based models which is an extension of Nataf's  
 119       joint distribution models (Nataf, 1962) initially implemented to generate random vec-  
 120       tors with arbitrary distributions in independent series but with cross-correlation. This  
 121       process starts with the generation of random data from Gaussian copulas to then trans-  
 122       form the marginal distribution with the inverse cumulative distribution function. The  
 123       SMARTA (Symmetric Moving Average (neaRly) To Anything) model (Tsoukalas et al.,  
 124       2018b) expands the capabilities of a Symmetric Moving Average (SMA), from just Gaus-  
 125       sian distribution to almost any distribution. The SMA models are able to replicate short-  
 126       run and long-run time dependencies in univariate as well as multivariate context, but  
 127       are unable to incorporate cyclostationary correlation structures (i.e., seasonality or pe-  
 128       riodicity in temporal correlation). A model which has several of the qualities of SMARTA  
 129       and is able to capture the cyclostationary correlation structure is SPARTA (Stochastic  
 130       Periodic AutoRegressive To Anything) (Tsoukalas et al., 2018a). SPARTA just as SMARTA  
 131       uses a Nataf-based model, but it starts with a PAR( $p$ ) model, instead of a SMA one. These  
 132       gives SPARTA the capability of simulating cyclostationary correlation, but it also loses  
 133       the capability of the SMARTA of simulating long-run time dependencies.

134       The long-run dependencies (LRD) are known as Hurst phenomenon (Koutsoyiannis,  
 135       2002), which is measured with the Hurst coefficient index ( $H$ ). The higher the magni-  
 136       tude of the index, the higher the prevalence of significant autocorrelation at very high  
 137       lags (e.g. 100 lags). A statistical model capable to capture and replicate the Hurst phe-  
 138       nomenon is the Fractional Gaussian Noise (FGN) method (Mandelbrot & Van Ness, 1968;  
 139       Mandelbrot & Wallis, 1968, 1969). The FGN was originally proposed as a mathemat-  
 140       ical approach to emulate long-range dependencies seen in normally distributed data, which  
 141       had immediate implications in hydrology. Unfortunately it was concluded that FGN fails  
 142       in simulations longer than 100 time periods (McLeod & Hipel, 1978). Although the FGN  
 143       can properly simulate the frequency of extreme events (Mandelbrot & Wallis, 1968), the  
 144       previously mentioned drawback was a dead end, until Kirsch et al. (2013) proposed the  
 145       modified Fractional Gaussian Noise (mFGN), and solved the period barrier that ham-

146 pered the use of FGN. The mFGN is able to generate univariate time series of infinite  
147 length, while replicating the cyclostationary correlation of it. With this model, Kirsch  
148 et al. (2013) demonstrated that one can use mFGN to simulate several years of stream-  
149 flow preserving its correlation structure. The streamflow generation with mFGN is per-  
150 formed by transforming the Gaussian generated data with a Log-Normal distribution.  
151 The method allows for additive changes in the mean and standard deviation of the time  
152 series, thereby making it a powerful and useful tool for climate variability and change  
153 studies. The mFGN approach has the advantage over autorregresive models, because it  
154 captures high levels of autocorrelation, cyclostationary correlation, as well as the Hurst  
155 phenomenon (Kirsch et al., 2013).

156 The mFGN proposed by Kirsch et al. (2013) has a good performance in replicat-  
157 ing a single-site streamflow, but, to the best of our knowledge, there is only one study  
158 that tries to extend mFGN to a multi-site context, without a successful result (Herman  
159 et al., 2016). Herman et al. (2016) increase the likelihood of drought events by increas-  
160 ing the weight of low streamflows in the distribution successfully. Nonetheless, they try  
161 to extend the mFGN into a multi-site method by using a bootstrap resampling technique  
162 of historical data, which is able to preserve historical temporal correlations, but it presents  
163 some difficulties in preserving spatial correlation. Although there are autorregresive multi-  
164 site models, in a single-site streamflow generation, the mFGN has shown to outperform  
165 autorregresive models such as AR( $p$ ) or PAR( $p$ ) (Kirsch et al., 2013), hence the exten-  
166 sion of mFGN into a multi-site method would allow preserving its benefits in multi-site  
167 streamflow generation.

168 Our main objective is to build a novel stochastic streamflow generator, which we  
169 call *Weighted-modified Fractional Gaussian Noise* (WmFGN), which is able to replicate  
170 historical time (i.e. short-run and long-run dependencies, as well as cyclostationary cor-  
171 relation) and space dependencies from the original data. The WmFGN is an extension  
172 of the mFGN into a multi-site method. WmFGN relies on the Cholesky decomposition  
173 of the spatial correlation matrix of the historical streamflow records, which is then used  
174 to add spatial correlation to streamflow time series simulated with mFGN. As the or-  
175 der in which the decomposition steps are performed (i.e., temporal then spatial, or vice-  
176 versa) affects the final result, our method searches for an optimal convex combination  
177 of the resulting matrices. The result is a Pareto-curve that indicates the optimal weights  
178 of the convex combination depending on the relative importance of spatial and tempo-

179 ral correlations given by the hydrological modeler. This framework represents an expan-  
 180 sion of the mFGN to the multi-streamflow case, which is useful for long term energy plan-  
 181 ning input, climate change assessment, water utility management, and other already proven  
 182 applications in which synthetic streamflow time series are required.

183 The paper is structured as follows. In Section 2 we present an in-depth explana-  
 184 tion of the proposed framework and its origins, moving on in Section 3 to a case study  
 185 in the Chilean Bio-bio river basin where the WmFGN is applied. The results are discussed  
 186 in Section 4, and Section 5 presents concluding remarks about the capabilities of the pro-  
 187 posed model.

## 188 2 Methodology

189 In this section we describe the *Weighted-mFGN* methodology we propose. Before  
 190 that, we recall the FGN and mFGN methodologies proposed in the literature, upon which  
 191 we build our approach. In what follows we shall assume that the monthly streamflow fol-  
 192 lows a log-normal distribution, which is a common assumption in the literature as stream-  
 193 flows do indeed tend to follow such a distribution in practice.

### 194 2.1 Fractional Gaussian Noise

195 We start by describing the Fractional Gaussian Noise (FGN) method (Mandelbrot  
 196 & Van Ness, 1968; Mandelbrot & Wallis, 1968, 1969). Consider a matrix  $\widehat{\mathbf{Y}}$  which is pop-  
 197 ulated with  $N$  years of historic inflow data in such a way that the hydrological years are  
 198 set as rows, and each month is a column (it is implied that months are treated as inde-  
 199 pendent processes  $\widehat{Y}_i^j = [\widehat{Y}_1^j, \dots, \widehat{Y}_N^j]$ , where the superscript  $j \in \{1, \dots, J\}$  stands for  
 200 the  $j$ th month, and the subscript  $i$  indexes the years in the data):

$$\widehat{\mathbf{Y}} = \begin{bmatrix} \widehat{\mathbf{Y}}_{1,1} & \widehat{\mathbf{Y}}_{1,2} & \widehat{\mathbf{Y}}_{1,3} & \cdots & \widehat{\mathbf{Y}}_{1,J} \\ \widehat{\mathbf{Y}}_{2,1} & \widehat{\mathbf{Y}}_{2,2} & \widehat{\mathbf{Y}}_{2,3} & \cdots & \widehat{\mathbf{Y}}_{2,J} \\ \widehat{\mathbf{Y}}_{3,1} & \widehat{\mathbf{Y}}_{3,2} & \widehat{\mathbf{Y}}_{3,3} & \cdots & \widehat{\mathbf{Y}}_{3,J} \\ \vdots & \vdots & \vdots & \ddots & \vdots \\ \widehat{\mathbf{Y}}_{N,1} & \widehat{\mathbf{Y}}_{N,2} & \widehat{\mathbf{Y}}_{N,3} & \cdots & \widehat{\mathbf{Y}}_{N,J} \end{bmatrix} \quad (1)$$

As a first step, the matrix  $\widehat{\mathbf{Y}}$  in (1) is transformed to resemble a Normal distribu-  
 tion in each of its months, and then it is standardized. More specifically, let  $\tilde{\mathbf{Y}}$  be de-

fined such that each element in  $\tilde{\mathbf{Y}}$  is the natural logarithm of  $\hat{\mathbf{Y}}$ . The means and variances corresponding to each month column in  $\tilde{\mathbf{Y}}$  (denoted by  $\tilde{\mu}_j$  and  $\tilde{\sigma}_j^2$ , respectively) are also calculated, consolidating a new whitened seasonality matrix  $\mathbf{Y}$  defined as follows:

$$\mathbf{Y}_{i,j} = \frac{\tilde{\mathbf{Y}}_{i,j} - \tilde{\mu}_j}{\tilde{\sigma}_j}, \quad i = 1, \dots, N, \quad j = 1, \dots, J. \quad (2)$$

The next step is to generate a new matrix  $\mathbf{X}$  of size  $N_s \times J$  with independent random samples from a  $\text{Normal}(0,1)$  distribution, where  $N_s$  is the number of years to simulate. This matrix  $\mathbf{X}$  is called the uncorrelated synthetic inflow matrix. To introduce the time dependencies of the original streamflow time-series, the matrix  $\Sigma := \text{Corr}(\mathbf{Y})$  is computed, which is the square and symmetric correlation matrix of the original rearranged time-series containing the pairwise correlation coefficients between all the months. The Cholesky decomposition of  $\Sigma$  is then computed as:

$$\Sigma = Q^T Q. \quad (3)$$

The Cholesky decomposition in (3) is the key step of the FGN because with the resulting upper triangular matrix  $Q$  the uncorrelated synthetic inflow matrix can be adjusted to capture the historic monthly temporal correlations, i.e. one computes

$$\mathbf{Z} := \mathbf{X}Q. \quad (4)$$

The output matrix  $\mathbf{Z}$  is of size  $N_s \times J$ . Note that  $\text{Corr}(\mathbf{Z}) \approx \text{Corr}(\mathbf{Y})$  as desired, thereby preserving the temporal correlation between months of each year, but not the correlations across years. Finally,  $\mathbf{Z}$  is transformed back into the original space of streamflows by computing

$$\bar{\mathbf{Z}}_{i,j} := \tilde{\mu}_j + \mathbf{Z}_{i,j} \tilde{\sigma}_j \quad (5)$$

$$\hat{\mathbf{Z}}_{i,j} := \exp(\bar{\mathbf{Z}}_{i,j}). \quad (6)$$

201

## 2.2 Modified Fractional Gaussian Noise (mFGN)

The FGN approach described above provides a clean and simple way to incorporate temporal correlations. One deficiency of the method, however, is that only considers the correlations between months *within the same year*. To overcome that issue, (Kirsch et al., 2013) propose a modification to the method that overlaps 6-month periods. More specifically, let  $\mathbf{Y}$  be the matrix constructed in (1). Then, a new matrix  $\mathbf{Y}'$

is built (see Figure 1a) so that the row corresponding to the  $i$ th year in  $\mathbf{Y}'$  contains the last six months of year  $i$  plus the first six months of year  $i+1$  in  $\mathbf{Y}$  (note that  $\mathbf{Y}'$  is one row shorter than  $\mathbf{Y}$ ). That is,  $\mathbf{Y}'$  can be constructed by applying a linear operator  $\mathcal{F}$  to  $\mathbf{Y}$  as follows. Let

$$\mathbf{T} := \begin{bmatrix} 0_{6 \times 6} & I_{6 \times 6} \\ I_{6 \times 6} & 0_{6 \times 6} \end{bmatrix} \quad (7)$$

and define the swapped data matrix  $\mathbf{S} := \mathbf{Y} \mathbf{T}$ . Define  $\mathbf{S}_1$  and  $\mathbf{S}_2$  as the left and right halves of  $\mathbf{S}$ , i.e.,

$$\mathbf{S} = [\mathbf{S}_1 | \mathbf{S}_2].$$

Now define the  $N - 1 \times N$  matrices

$$\mathbf{I}_1 := \begin{bmatrix} 1 & 0 & 0 & \dots & 0 & 0 \\ 0 & 1 & 0 & \dots & 0 & 0 \\ \vdots & & & & & \\ 0 & 0 & 0 & \dots & 1 & 0 \end{bmatrix} \quad \text{and} \quad \mathbf{I}_2 := \begin{bmatrix} 0 & 1 & 0 & \dots & 0 \\ 0 & 0 & 1 & \dots & 0 \\ \vdots & & & & \\ 0 & 0 & 0 & \dots & 1 \end{bmatrix}.$$

Then we have that

$$\mathbf{Y}' = \mathcal{F}(\mathbf{Y}) := [\mathbf{I}_1 \mathbf{S}_1 | \mathbf{I}_2 \mathbf{S}_2].$$

Let  $Q'$  be the matrix corresponding to the Cholesky decomposition of  $\text{Corr}(\mathbf{Y}')$ .

Now, consider as before a matrix  $\mathbf{X}$  of size  $N_s \times J$  with independent random samples from a  $\text{Normal}(0,1)$  distribution, where  $N_s$  is one year more than the ones to be simulated, and the matrix  $Q$  corresponding to the Cholesky decomposition of  $\text{Corr}(\mathbf{Y})$ . Then, a new matrix  $\mathbf{X}'$  of size  $N_s - 1 \times J$  is constructed by applying the linear operator  $\mathcal{F}$  defined above to  $\mathbf{X}$ , i.e.,  $\mathbf{X}' := \mathcal{F}(\mathbf{X})$ , and one computes

$$\mathbf{Z}^1 := \mathbf{X}Q, \quad \mathbf{Z}^2 := \mathbf{X}'Q'. \quad (8)$$

The final matrix  $\mathbf{Z}$  of simulated values is then built by using the right-most columns of  $\mathbf{Z}^1$  and  $\mathbf{Z}^2$ , as indicated in Figure 1b.

### 2.3 Weighted modified Fractional Gaussian Noise (WmFGN)

#### 2.3.1 Spatial correlation integration into temporally correlated data

The mFGN method described above yields excellent results in the sense that the corresponding simulated series preserve the temporal correlation of the data. The method, however, falls short of representing *spatial* correlations adequately. To circumvent this

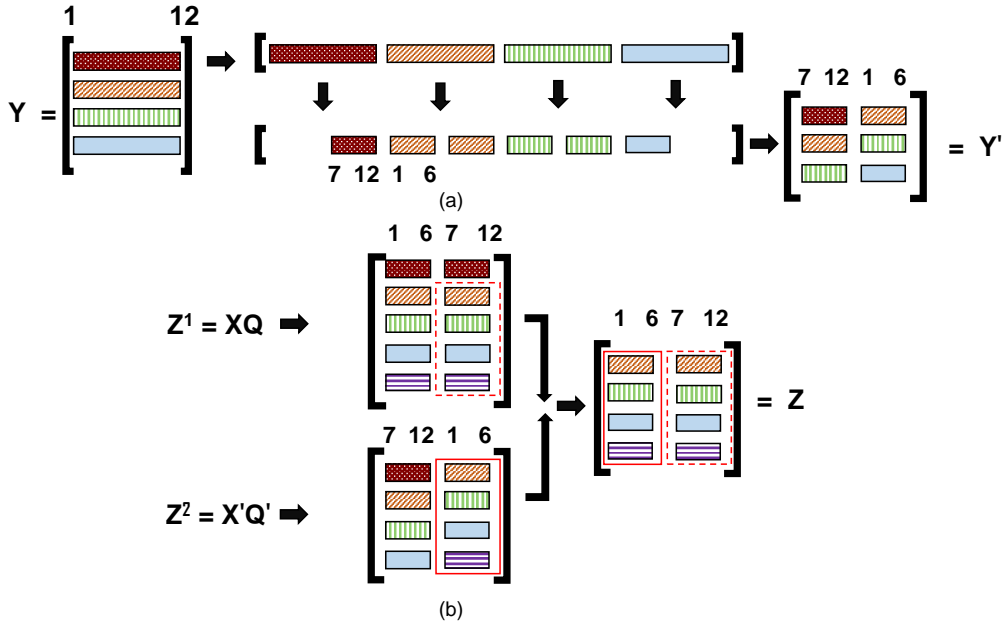


**Figure 1.** (a) Example process of how to retrieve  $\mathbf{Y}'$  out of  $\mathbf{Y}$  matrix (equivalent to the obtention of  $\mathbf{X}'$  out of  $\mathbf{X}$ ). (b) Demonstration of how to build  $\mathbf{Z}$ . Monthly scaled version of the mFGN process developed in Kirsch et al. (2013)

limitation, Kirsch et al. (2013) propose a modification that uses the same random “seed” when simulating correlated basins. The spatial approach proposed by Kirsch et al. (2013) consists in applying the mFGN as described in Section 2.2, but with a slight modification when building  $\mathbf{X}$ . Instead of using random  $\text{Normal}(0,1)$  numbers to fill  $\mathbf{X}$ , one *bootstraps* values from the historical data  $\mathbf{Y}$ . That is, for each month/year one wants to simulate, a year is selected randomly from the historical data and the corresponding month of that year is used for  $\mathbf{X}$ . The spatial correlation is then imposed by making sure the historical bootstrapped seed corresponds to the same month and year in each site.

To illustrate the idea, suppose we want to generate simulated values for the months of January, February and March in the year 2025 at two nearby sites, and that  $\mathbf{Y}$  contains the monthly records of both sites from 1981 to 2020. Then, a random selection of years for  $\mathbf{X}$  might choose 1992, 2005, and 1987 for January, February and March, respectively, and the corresponding  $\mathbf{Y}$  values of those months/years are used for *both* sites. That is, by denoting by  $\mathbf{X}_{i,j}^k$  the simulated streamflow for month  $j$  of year  $i$  at site  $k$  (and sim-

ilarly for the historical data  $\mathbf{Y}$ ) we have:

$$\begin{aligned}\mathbf{X}_{2025,1}^1 &:= \mathbf{Y}_{1992,1}^1, & \mathbf{X}_{2025,1}^2 &:= \mathbf{Y}_{1992,1}^2 \\ \mathbf{X}_{2025,2}^1 &:= \mathbf{Y}_{2005,2}^1, & \mathbf{X}_{2025,2}^2 &:= \mathbf{Y}_{2005,2}^2 \\ \mathbf{X}_{2025,3}^1 &:= \mathbf{Y}_{1987,3}^1, & \mathbf{X}_{2025,3}^2 &:= \mathbf{Y}_{1987,3}^2\end{aligned}$$

218 Note that each site will have its own set of simulated values  $\mathbf{X}$ , but the values will be  
 219 correlated because the historical data is spatially correlated. Nevertheless, the mFGN  
 220 distorts the spatial correlation as reported by Herman et al. (2016). Because of the lim-  
 221 itations of mFGN in preserving spatial correlation, we propose an alternative method,  
 222 as we describe next.

To introduce spatial correlation to the independently simulated streamflows of each site, we shall consider a three-dimensional version of the normalized historical inflow data matrix  $\mathbf{Y}$  defined in (1)-(2) so that the third dimension corresponds to each site (see Figure 2). Denote the new structure as  $\mathcal{Y}$ , which has dimension  $N \times J \times K$ , where  $K$  is the total number of sites and denote by  $\mathbf{Y}^k$  the normalized historical inflow data matrix for site  $k$ . We then have that  $\mathcal{Y} = [\mathcal{Y}_{ijk}]$ , where

$$\mathcal{Y}_{ijk} := \mathbf{Y}_{i,j}^k, \quad i = 1, \dots, N, \quad j = 1, \dots, J, \quad k = 1, \dots, K. \quad (9)$$

The main idea of our procedure is described as follows. First, we create matrices  $\mathbf{U}^1, \dots, \mathbf{U}^J$ , each of dimension  $N \times K$ , such that each  $\mathbf{U}^j$ ,  $j = 1, \dots, J$ , is a slice of  $\mathcal{Y}$  *in the dimension of time*, i.e.,  $\mathbf{U}^j = [\mathbf{U}_{ik}^j]$ , where

$$\mathbf{U}_{ik}^j := \mathcal{Y}_{i,j,k}, \quad i = 1, \dots, N, \quad k = 1, \dots, K. \quad (10)$$

As a second step, we calculate the spatial correlation matrix  $\text{Corr}(\mathbf{U}^j)$  and its upper triangular Cholesky decomposition matrix  $R^j$  (of dimension  $K \times K$ ), i.e.,

$$(R^j)^T(R^j) = \text{Corr}(\mathbf{U}^j). \quad (11)$$

Next, we construct a three-dimensional matrix  $\mathcal{Z}$  similarly to  $\mathcal{Y}$ , but using the matrices  $\mathbf{Z}^k$  of *simulated* data constructed in Section 2.2 for each site  $k$  instead of the normalized data matrices  $\mathbf{Y}^k$ . As before, we define matrices  $\mathbf{V}^1, \dots, \mathbf{V}^J$ , each of dimension  $N_s \times K$ , such that each  $\mathbf{V}^j$ ,  $j = 1, \dots, J$ , is a slice of  $\mathcal{Z}$  in the dimension of time, i.e..

$$\mathbf{V}_{ik}^j := \mathcal{Z}_{i,j,k}, \quad i = 1, \dots, N_s, \quad k = 1, \dots, K. \quad (12)$$

The key step of our procedure is the calculation of the matrices

$$\mathbf{W}^j := \mathbf{V}^j R^j, \quad j = 1, \dots, J. \quad (13)$$

Such a step incorporates the spatial correlation into the simulated data for each month.

Finally, we construct a three-dimensional matrix  $\mathcal{W}$  as

$$\mathcal{W}_{ijk} := \mathbf{W}_{i,k}^j, \quad i = 1, \dots, N_s, \quad j = 1, \dots, J, \quad k = 1, \dots, K. \quad (14)$$

The matrix  $\mathcal{W}$  now contains our simulated data for all sites and all months, which takes into account both temporal and spatial correlations, *in that order*. We shall call this procedure *mFGNS*, which is illustrated in Figure 2.

**2.3.2 Reverting the order: temporal correlation integration into spatially correlated data**

The mFGNS procedure proposed in Section 2.3.1 makes clear that spatial correlation is incorporated into the simulated data *after* accounting for temporal correlation. One could, however, invert the order in which we apply the correlations. That is, starting with the full normalized data matrix  $\mathcal{Y}$  constructed in (9), we can first construct matrices  $\mathbf{U}^1, \dots, \mathbf{U}^J$  as in (10) and their respective Cholesky decomposition matrices  $R^j$  as in (11). The next step is to generate a new matrix  $\tilde{\mathbf{X}}$  of size  $N_s \times K$  with independent random samples from a  $\text{Normal}(0,1)$  distribution, where  $N_s$  is the one year more than the number of years to simulate. Now, by using the Cholesky decomposition matrix  $R^j$ , the uncorrelated synthetic matrix  $\tilde{\mathbf{X}}$  can be adjusted to capture the spatial correlation for each month  $j$ , i.e. one computes

$$\tilde{\mathbf{V}}^j := \tilde{\mathbf{X}} R^j. \quad (15)$$

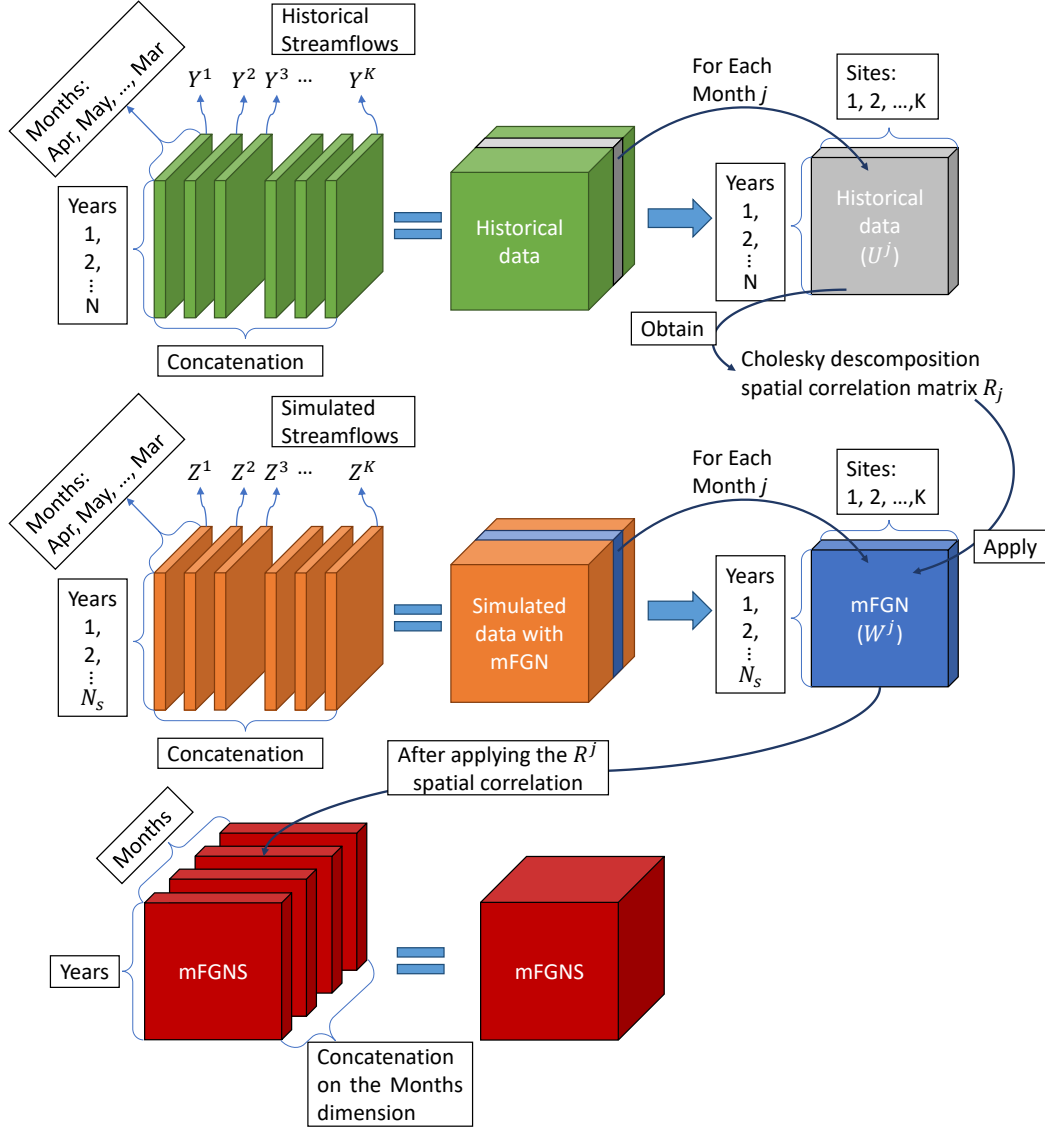
Note that  $\tilde{\mathbf{V}}^j$  (which has dimension  $N_s \times K$ ) contains the spatially correlated simulated data for month  $j$ . We then construct the three-dimensional matrix  $\tilde{\mathcal{V}}$  as

$$\tilde{\mathcal{V}}_{ijk} := \tilde{\mathbf{V}}_{i,k}^j, \quad i = 1, \dots, N_s, \quad j = 1, \dots, J, \quad k = 1, \dots, K, \quad (16)$$

and define  $\tilde{\mathbf{Z}}^1, \dots, \tilde{\mathbf{Z}}^K$ , each of dimension  $N_s \times J$  as slices of  $\tilde{\mathcal{V}}$  *in the dimension of space*, i.e., for each  $k = 1, \dots, K$  we have

$$\tilde{\mathbf{Z}}_{ij}^k := \tilde{\mathcal{V}}_{i,j,k}, \quad i = 1, \dots, N_s, \quad j = 1, \dots, J. \quad (17)$$

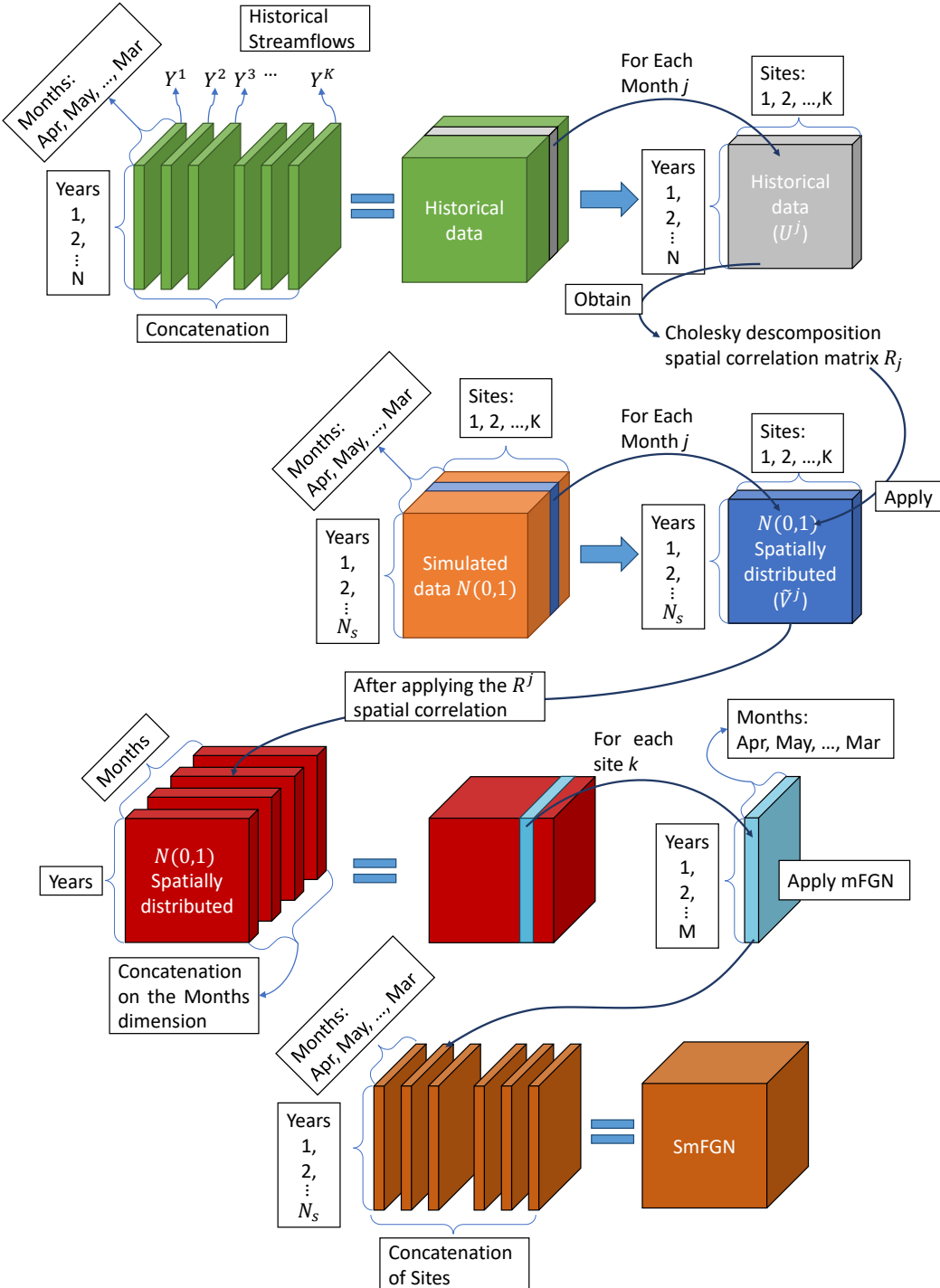
Then, for each  $k = 1, \dots, K$ , we apply the mFGN procedure of Section 2.2 with  $\tilde{\mathbf{Z}}^k$  in place of  $\mathbf{X}$ , thereby yielding a matrix  $\tilde{\mathbf{W}}^k$  which incorporates temporal correlation into

**Figure 2.** Schematics of mFGNS

the (spatially correlated) simulated data for site  $k$ . Finally, we construct a three-dimensional matrix  $\tilde{\mathcal{W}}$  as

$$\tilde{\mathcal{W}}_{ijk} := \tilde{\mathbf{W}}_{i,j}^k, \quad i = 1, \dots, N_s, \quad j = 1, \dots, J, \quad k = 1, \dots, K. \quad (18)$$

The matrix  $\tilde{\mathcal{W}}$  now contains our simulated data for all sites and all months, which takes into account both spatial and temporal correlations, *in that order*. We shall call this procedure *SmFGN*, which is illustrated in Figure 3.

**Figure 3.** Schematics of SmFGN

231      **2.3.3 Combining the mFGNS and SmFGN approaches**

232      As discussed earlier, the procedures mFGNS and SmFGN described in the previ-  
 233      ous sections both aim at the same goal, which is to incorporate spatial correlation into  
 234      the mFGN approach. The two procedures, however, lead to different simulated results,  
 235      as the order in which the spatial and temporal correlations are considered does indeed  
 236      matter. As we shall see in Section 4, the dimension that is considered first (spatial or  
 237      temporal) is worse represented in the simulated data than the dimension that comes sec-  
 238      ond.

It is natural then to consider a *weighted average* of the simulated data generated by the two procedures, a procedure we shall call *Weighted mFGN* (WmFGN for short). Note that for the WmFGN procedure to work, the random numbers  $\mathbf{X}$  used in the mFGNS and SmFGN procedures must be the same. More specifically, we consider the three-dimensional matrices  $\mathcal{W}$  and  $\widetilde{\mathcal{W}}$  defined respectively in (14) and (18), and define, for  $\alpha \in [0, 1]$ ,

$$\widehat{\mathcal{W}}(\alpha) := (1 - \alpha)\mathcal{W} + \alpha\widetilde{\mathcal{W}}. \quad (19)$$

Our goal is to find the value of  $\alpha$  such that the spatial and temporal correlations induced by  $\widehat{\mathcal{W}}(\alpha)$  are closest to the corresponding correlations of the historical data. With that in mind, we define the following error metrics:

$$\Delta_{\text{avg}}^s(\alpha) := \text{mean spatial error} = \frac{1}{J} \sum_{j=1}^J \frac{1}{K^2} \sum_{\ell,k=1}^K \left| \text{Corr}(\mathbf{Y}^j)_{\ell k} - \text{Corr}(\widehat{\mathbf{W}}^j(\alpha))_{\ell k} \right|, \quad (20)$$

$$\Delta_{\text{avg}}^t(\alpha) := \text{mean temporal error} = \frac{1}{K} \sum_{k=1}^K \frac{1}{J^2} \sum_{j,\ell=1}^J \left| \text{Corr}(\mathbf{Y}^k)_{j\ell} - \text{Corr}(\widehat{\mathbf{W}}^k(\alpha))_{j\ell} \right|, \quad (21)$$

$$\Delta_{\text{max}}^s(\alpha) := \text{max. spatial error} = \max_{j=1,\dots,J} \max_{\ell,k=1,\dots,K} \left| \text{Corr}(\mathbf{Y}^j)_{\ell k} - \text{Corr}(\widehat{\mathbf{W}}^j(\alpha))_{\ell k} \right|, \quad (22)$$

$$\Delta_{\text{max}}^t(\alpha) := \text{max. temporal error} = \max_{k=1,\dots,K} \max_{j,\ell=1,\dots,J} \left| \text{Corr}(\mathbf{Y}^k)_{j\ell} - \text{Corr}(\widehat{\mathbf{W}}^k(\alpha))_{j\ell} \right|. \quad (23)$$

239      In the above equations,  $\mathbf{Y}^j$  denotes a slice of  $\mathcal{Y}$  across the month  $j$ ,  $\mathbf{Y}^k$  denotes a slice  
 240      of  $\mathcal{Y}$  across the site  $k$ , and similarly for  $\widehat{\mathbf{W}}^j(\alpha)$  and  $\widehat{\mathbf{W}}^k(\alpha)$ .

The metrics defined in (20)-(23) measure the correlation error in four different ways—spatial or temporal error, mean or maximum error. Suppose the decision maker is interested in minimizing both the spatial and temporal errors, but one of the dimensions is more important than the other. Such preference can be represented by a (user-defined) parameter  $\lambda \in [0, 1]$  such that the temporal error has weight  $\lambda$  whereas the spatial error has weight  $1 - \lambda$ . We can then define two optimization problems to find the opti-

mal  $\alpha$ :

$$\text{Objective 1: } \min_{\alpha \in [0,1]} \lambda \Delta_{\text{avg}}^t(\alpha) + (1 - \lambda) \Delta_{\text{avg}}^s(\alpha) \quad (24)$$

$$\text{Objective 2: } \min_{\alpha \in [0,1]} \lambda \Delta_{\text{max}}^t(\alpha) + (1 - \lambda) \Delta_{\text{max}}^s(\alpha). \quad (25)$$

Note that, in either case, the optimal  $\alpha^*$  is a function of the user-defined parameter  $\lambda$ .

Once  $\alpha^*$  is found, by using (19) the simulated data is then defined as  $\widehat{\mathcal{W}}(\alpha^*)$ .

**Remark:** The metrics defined in (20)-(23) can be interpreted in terms of vector norms on matrices (see, e.g., Horn and Johnson (2012)). To see that, given a square matrix  $A_{M \times M}$ , for  $p \geq 1$  define the  $\ell_p$ -norm

$$\|A\|_p := \left( \sum_{i=1}^M \sum_{j=1}^M |A_{ij}|^p \right)^{1/p}.$$

As customary, the above definition can be extended to  $p = \infty$  as follows:

$$\|A\|_\infty := \max_{i=1,\dots,M} \max_{j=1,\dots,M} |A_{ij}|.$$

Define now the following error metrics:

$$\Delta_p^s(\alpha) := \text{spatial error} = \left\| \left[ v_j : v_j = \left\| \text{Corr}(\mathbf{Y}^j) - \text{Corr}(\widehat{\mathbf{W}}^j(\alpha)) \right\|_p \right] \right\|_p, \quad (26)$$

$$\Delta_p^t(\alpha) := \text{temporal error} = \left\| \left[ u_k : u_k = \left\| \text{Corr}(\mathbf{Y}^k) - \text{Corr}(\widehat{\mathbf{W}}^k(\alpha)) \right\|_p \right] \right\|_p, \quad (27)$$

In the above equations,  $\mathbf{Y}^j$  denotes a slice of  $\mathcal{Y}$  across the month  $j$ ,  $\mathbf{Y}^k$  denotes a slice of  $\mathcal{Y}$  across the site  $k$ , and similarly for  $\widehat{\mathbf{W}}^j(\alpha)$  and  $\widehat{\mathbf{W}}^k(\alpha)$ . We see that (26)-(27) coincides with (22)-(23) when  $p = \infty$ . Moreover, when  $p = 1$ , (20) is equivalent to (26) divided by  $JK^2$ , whereas (21) is equivalent to (27) divided by  $KJ^2$ . We use (20)-(23) as they are more intuitive to formulate, but the interpretation as vector norms on matrices opens the possibility to measure the error with different values of  $p$ —for instance,  $p = 2$  which corresponds to the well-known Frobenius norm.

In the next sections we present a case study to illustrate the application of the WmFGN procedure described above, and compare the results with those obtained by using the approach of (Kirsch et al., 2013).

253      **3 Case study**

254      To test the *WmFGN* methodology, we simulate streamflows from the Bio-bio river  
 255      basin depicted in Figure 4. The Bio-bio river basin, located in Southern Chile, presents  
 256      an average annual precipitation of 1,330 mm, which leads to mean daily discharges of  
 257       $960 \text{ m}^3/\text{s}$  (Grantham et al., 2013). The basin has a significant urban area, which in-  
 258      cludes the city of Concepción, a large percentage of forest plantations ( $\sim 20\%$  of the land  
 259      cover), and has been historically important for the country due to its hydroelectric pro-  
 260      duction (Grantham et al., 2013). The Bio-bio river basin represents almost 40% of the  
 261      hydroelectric potential of Chile, a country that is historically known for the importance  
 262      of its hydroelectric sector (CNE, 2023). In addition, the Biobio region (i.e., formed by  
 263      the Biobio basin, small coastal basins near Biobio and also used to include the north-  
 264      ern Ñuble region, see Figure 4) supplies about 10% of Chile's urban drinking water con-  
 265      sumption (Molinos-Senante & Donoso, 2021).

266      Given the importance of hydroelectricity for Chile and the Bio-bio river basin, we  
 267      decided to perform our numerical analysis on the streamflows of that basin used by the  
 268      National Electric Coordinator (NEC) (CEN, 2021). The data includes weekly stream-  
 269      flows (i.e., considering four weeks per month) between the hydrological years 1960/61  
 270      and 2018/19, note that hydrological years start in April in this region, of the rivers of  
 271      interest for the NEC (e.g. inflows of hydro-power plants). After filtering the NEC stream-  
 272      flow database by location, the weekly flows were aggregated into monthly time series.  
 273      Then, the flows were filtered to identify those for which most of their months (i.e., at least  
 274      9 out of 12) had a log-normal distribution. Finally, nine sites remained for the Bio-bio  
 275      river basin, which are those presented in Figure 4. Statistics for these rivers are presented  
 276      in Table 1, which include location, annual streamflow mean and standard deviation.

277      The seasonal variation of the monthly mean and standard deviation of the stream-  
 278      flows, for the period 1960/61-2018/19, are presented in Figures 5 for three representa-  
 279      tive rivers (Abanico, El Toro and Ralco). Seasonal variations for the remaining six rivers  
 280      are given in the Supplementary material (Figures S1 and S2). As can be seen in these  
 281      figures, most locations, regardless of the streamflows magnitudes, present a double peak  
 282      in the Winter months (Jun-July) and in Spring (October to December). The first one  
 283      is related to a pluvial peak, given that most of the precipitation falls during Winter, while

284 the second peak is related to snow-melt. Hence, the Bio-bio river basins has a mixed nivo-  
285 pluvial flow.

286 Some recent challenges of the Bio-bio river basin have been related to both floods  
287 and droughts. Hence, developing proper hydrological modeling is of importance for the  
288 basin. The Bio-bio river basin suffered a 100-year flood during Winter of 2006 (Gironás  
289 et al., 2021). On the other hand Bio-bio is undergoing a “megadrought”, which corre-  
290 sponds to an uninterrupted event of below-average precipitation years since 2010 (Boisier  
291 et al., 2016). The megadrought is a phenomenon that has affected other basins as well  
292 (Barría et al., 2021), having an impact for more than a decade over Central-Southern  
293 Chile (Garreaud et al., 2020, 2021). Also, climate change projections over Central-Southern  
294 Chile indicate that precipitations should decrease in the future (Chadwick et al., 2018;  
295 Araya-Osses et al., 2020; Chadwick et al., 2023).

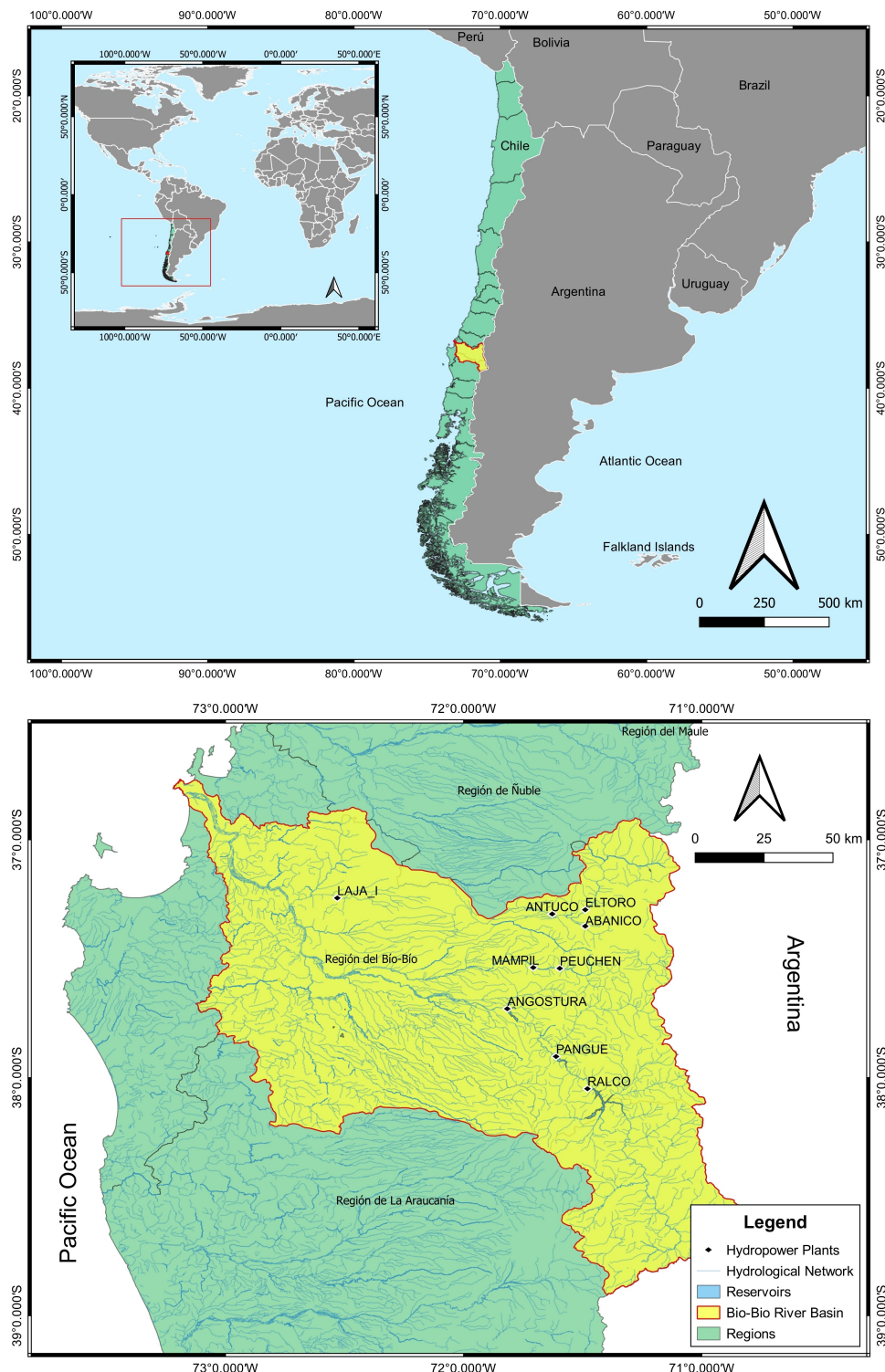


**Table 1.** Locations of the streamflows with their annual mean, and standard deviation

Site Number	River	Lat.	Lon.	Mean ( $m^3/s$ )	Std. Dev. ( $m^3/s$ )
1	Laja I	-37.24	-72.53	15.09	6.96
2	Angostura	-37.71	-71.81	131.49	39.46
3	Antuco	-37.31	-71.63	49.05	15.07
4	Abanico	-37.36	-71.50	4.46	1.46
5	El Toro	-37.29	-71.50	61.67	16.61
6	Ralco	-38.04	-71.48	249.45	68.92
7	Pangue	-37.91	-71.61	28.17	11.49
8	Mampil	-37.53	-71.70	21.75	5.31
9	Peuchen	-37.54	-71.59	35.50	9.17

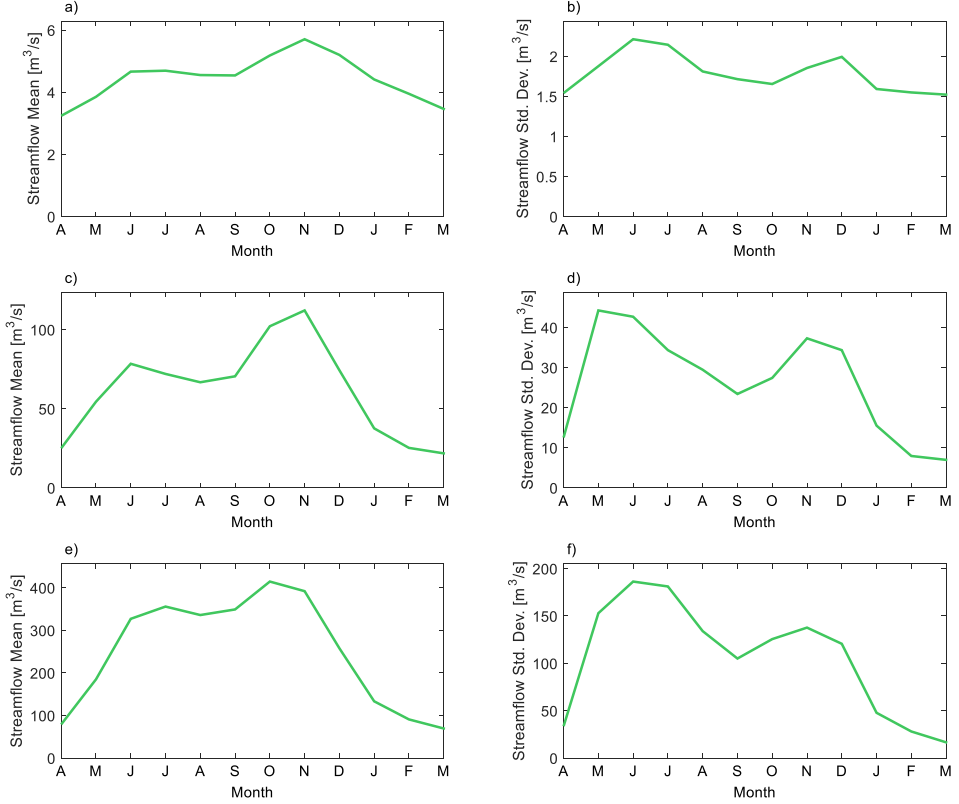


**Figure 5.** Monthly mean (a, c, and e) and standard deviation (b, d, and f) of the streamflows of Abanico (a, and b), El Toro (c, and d), and Ralco (e, and f) rivers.

296

## 4 Numerical results

297

### 4.1 Optimal parameters from WmFGN

298  
299  
300  
301  
302  
303  
304  
305  
306

The performance of the proposed WmFGN is measured in term of its capability of preserving the original temporal and spatial correlations in the observed data. The measurements of correlation errors of the simulated data are computed in Eqs. (20) to (23) for different values of  $\alpha$  and plotted in Figures 6a and 6b. The performance is also compared against that of the mFGN, which is not dependent on  $\alpha$  and presents difficulties with replicating the spatial correlation of the observed data. The temporal and spatial correlation errors for the mean and maximum error metrics for mFGN are computed using similar expressions as in (20)-(23), but with the matrix  $\widehat{W}(\alpha)$  replaced with the matrix corresponding to the mFGN method with spatial correlation added via re-sampling,

307 as discussed in Section 2.3.1. We shall denote the resulting correlation errors for mFGN  
 308 by  $\delta_{\text{avg}}^s$ ,  $\delta_{\text{avg}}^t$ ,  $\delta_{\text{max}}^s$  and  $\delta_{\text{max}}^t$ , using a notation analogous to that in (20)-(23).

309 Figures 6c and 6d depict the Pareto frontier of spatial and temporal correlation er-  
 310 rors. As expected, there is a trade-off between obtaining good performance in the spa-  
 311 tial correlation and good performance in the temporal correlation, both in terms of the  
 312 mean error (Figures 6a and 6c) and the maximum error (Figures 6b and 6d).

313 For this specific problem, we see in Figures 6b and 6d that the WmFGN, with a  
 314 value of  $\alpha$  around 0.5, shows considerable reduction of the maximum error in the spa-  
 315 tial correlation compared to mFGN (which coincides with the spatial error of WmFGN  
 316 with  $\alpha = 1$ ), with almost no increase in the temporal correlation error. On the other  
 317 hand, we observe in Figures 6a and 6c that there is a range of values of  $\alpha$  (between around  
 318 0.75 and 0.98) for which both spatial and temporal mean errors for WmFGN are smaller  
 319 than the mFGN errors, that is, for that metric WmFGN is superior to mFGN in both  
 320 spatial and temporal dimensions.

321 Although the results are specific for the Bio-bio basin, they represent a clear illus-  
 322 tration of how the WmFGN presents an improvement over mFGN in terms of preserv-  
 323 ing both spatial and temporal correlations, in addition to allowing for more flexibility.

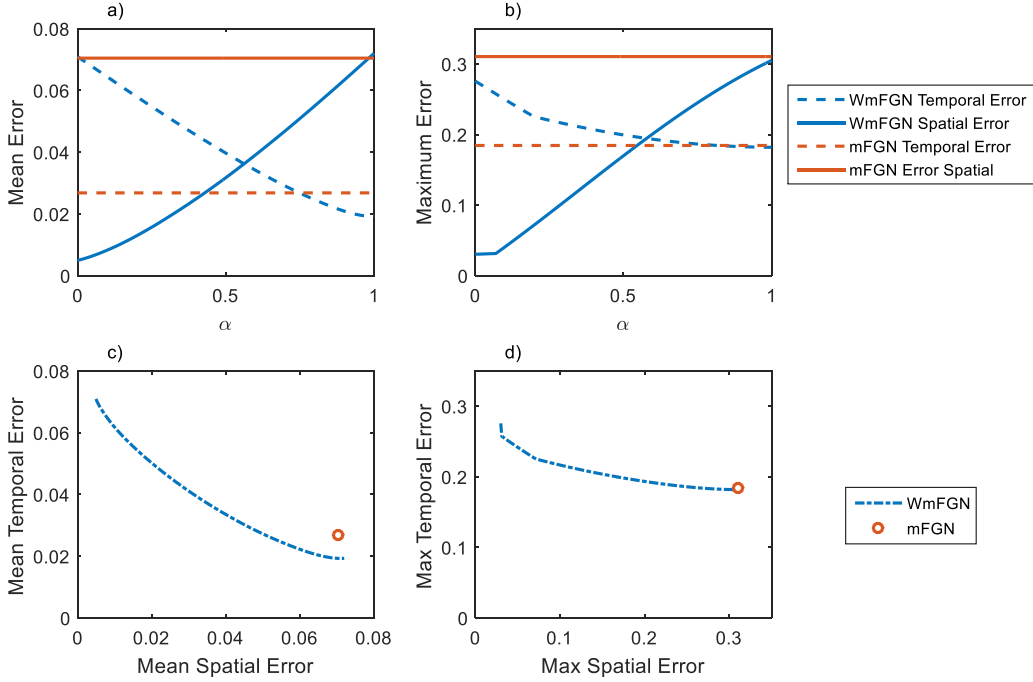


**Figure 6.** Mean (a) and maximum (b) spatial and temporal correlation errors as a function of  $\alpha$ ; (c) and (d) depict spatial vs. temporal error for the mean and maximum error metrics, respectively.

When finding the optimal weight  $\alpha$  balancing mFGNS and SmFGN in (19) that minimizes the weighted sum of spatial and temporal mean (resp. maximum) correlation errors with model (24) (resp. (25)) under different user-defined parameters  $\lambda$ , we obtain a curve as displayed in Figure 7a (resp. Figure 7b). As discussed earlier, the value of  $\lambda$  allows the user of WmFGN to prioritize between the spatial (i.e.,  $\lambda=0$ ) or temporal (i.e.,  $\lambda=1$ ) correlation. Not surprisingly, the optimal value of  $\alpha$  coincides with  $\lambda$  at the extreme cases—after all, if the user is only concerned with spatial correlation (i.e., chooses  $\lambda = 0$ ) then the best combination between mFGNS and SmFGN is really just using mFGNS which gives the highest priority to spatial correlation, and that corresponds to taking  $\alpha = 0$  in (19). An analogous argument holds for the case where temporal correlation is preferred.

The optimal values of the objective functions 1 (Eq. (24)) and 2 (Eq. (25)) are presented in Figures 7c and 7d, respectively, for different values of the user-defined parameter  $\lambda$ . For comparison, we also compute the values of Objectives 1 and 2 for the mFGN.

This amounts to calculating

$$\text{Objective 1: } \lambda\delta_{\text{avg}}^t + (1 - \lambda)\delta_{\text{avg}}^s \quad (28)$$

$$\text{Objective 2: } \lambda\delta_{\text{max}}^t + (1 - \lambda)\delta_{\text{max}}^s, \quad (29)$$

where  $\delta_{\text{avg}}^t$ ,  $\delta_{\text{avg}}^s$ ,  $\delta_{\text{max}}^t$  and  $\delta_{\text{max}}^s$  are the correlation errors for mFGN, as defined earlier.

Note that for objective function 1, WmFGN always yields lower values than mFGN (Figure 7c), whereas for objective function 2, WmFGN yields lower values than mFGN for most values of  $\lambda$ , except when  $\lambda$  is close to 1 in which case both WmFGN and mFGN coincide (Figure 7d). The advantage of using WmFGN over mFGN increases as the user gives higher importance of spatial correlation over temporal one, which is visually represented as the increasing gap between the objective functions in Figures 7c and 7d, as  $\lambda$  approaches zero.

Deciding on an appropriate value for  $\lambda$  will depend on the user's priority for correctly simulating spatial or temporal correlation, which will eventually define the associated value for  $\alpha$ . Nevertheless, if the user has similar priorities for both correlations, and wants to decide which  $\lambda$  to use, an option could be simply using  $\lambda=0.5$ . Interestingly, as seen in Figure 7a, such a value corresponds to taking  $\alpha = 0.33$ , that is, giving twice the weight to mFGNS relatively to SmFGN. Another option could be equating the temporal and spatial errors, which for the mean error criterion yields a value of  $\alpha$  of 0.562 (Figure 6a), whereas for the maximum error criterion it yields a value of  $\alpha = 0.578$  (Figure 6b). These values of  $\alpha$  correspond to taking  $\lambda = 0.574$  and  $\lambda = 0.842$  for the mean and maximum error criteria, respectively (Figure 7a and 7b). Note also that these values of  $\lambda$  are the maximizers of the WmFGN objective functions in Figures 7c and 7d, and represent a change in the concavity of the  $\alpha$ -curves (Figures 7a and 7b).

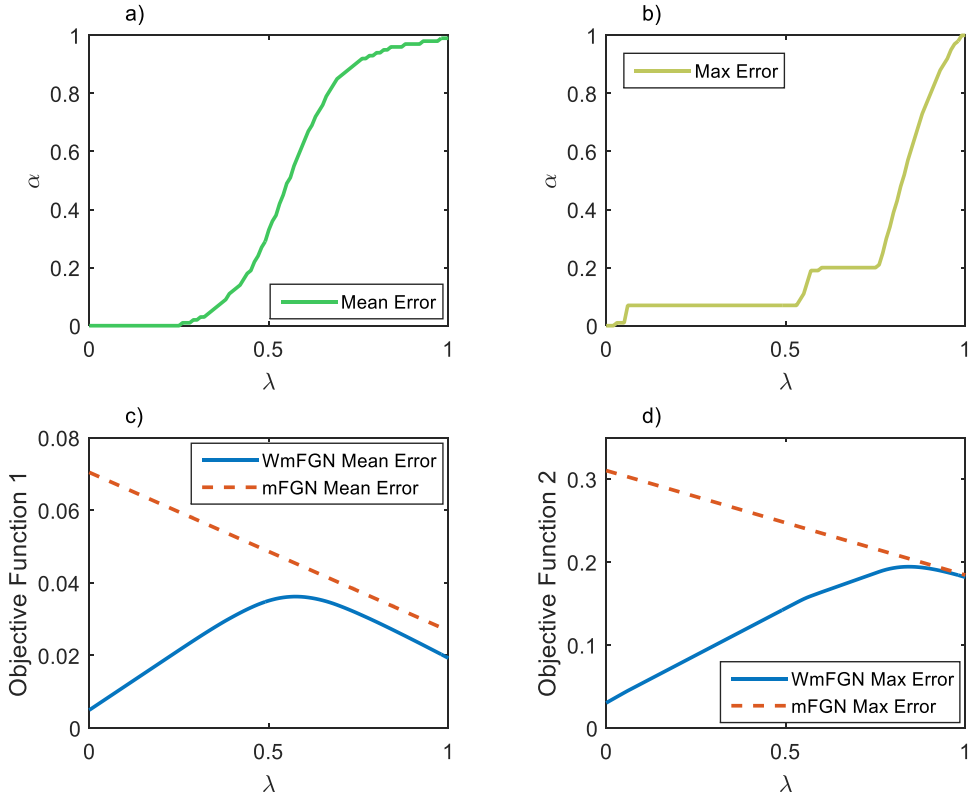


**Figure 7.** Optimal values of  $\alpha$  as a function of  $\lambda$  for the mean error (a) and maximum error (b) criteria; (c) and (d) depict the optimal objective function values in (24) and (25), respectively, as a function of  $\lambda$ .

#### 4.2 Illustration of the behaviour of the correlations

One advantage of the WmFGN approach, compared to other methods proposed in the literature (including mFGN) is that it tailors the procedure according to the importance of temporal vs spatial correlation specified by the user, which in this case is accomplished by means of the parameter  $\lambda$  in (24) and (25). Figures 8d-8h and 9d-9h illustrate that flexibility, displaying the correlations calculated from the simulated data generated by WmFGN using the mean error metric (Objective 1). The figures depict the temporal correlation of among months for a representative river (Ralco), and the spatial correlation among locations for a representative month (November), respectively, for different values of the parameter  $\lambda$ . In addition to the actual correlations, Figures 8i-8m and 9i-9m show the correlation errors with respect to observed data. For the sake of comparison, Figures 8a-8c and 9a-9c show the correlations of observed data, the cor-

367 relations calculated from data simulated for mFGN, and the associated correlation er-  
 368 rors.

369 The figures demonstrate that WmFGN accomplishes what it proposes to do. For  
 370 values of  $\lambda \geq 0.75$  (priority to temporal correlation), we see in Figure 8 that the tem-  
 371 poral correlation errors are indeed small. These errors increase as  $\lambda$  decreases. In Fig-  
 372 ure 9 we see the opposite effect—the spatial errors are small for  $\lambda \leq 0.25$  (priority to  
 373 spatial correlation), and increase as  $\lambda$  increases.

374 The figures also corroborate the previous conclusions about the benefit of the Wm-  
 375 FGN approach over mFGN for preserving both spatial and temporal correlations. The  
 376 mFGN procedure—which by construction prioritizes temporal correlation—presents very  
 377 low temporal correlation errors as shown in Figure 8c, at the expense of high spatial cor-  
 378 relation errors (see Figure 9c). This is in line with the results of previous studies (Herman  
 379 et al., 2016). However, a comparison between the correlation errors for mFGN and for  
 380 WmFGN with  $\lambda = 1$  in Figures 8m and 9m (which is the comparable case where full  
 381 priority is given to temporal correlation) shows that the temporal correlation errors for  
 382 WmFGN are in fact smaller than those for mFGN, and the spatial correlation errors are  
 383 similar. Moreover, by introducing flexibility via the  $\lambda$  parameter, the WmFGN approach  
 384 allows the user to “sacrifice” some of the precision in the temporal correlation in order  
 385 to increase the precision in the spatial correlation—a flexibility that is not present in mFGN.

386 The above discussion is based on the results corresponding to Objective 1 (mean  
 387 error criterion). Similar conclusions can be obtained by examining Figures 10 and 11,  
 388 which display the results corresponding to Objective 2 (maximum error criterion). Note  
 389 also that the results discussed above for the chosen representative river and month ap-  
 390 pply similarly to the other rivers and months considered in this paper as shown in Fig-  
 391 ures S3 to S40 in the Supplementary Material.

392 Although the choice of error metric to be used (mean or maximum error, correspond-  
 393 ing to Objective 1 and 2, respectively) is problem-specific and depends on the priorities  
 394 of the user, there are some general recommendations. For example, when comparing the  
 395 WmFGN temporal correlation errors in Figures 8i-8m and 10i-10m, we see that the lat-  
 396 ter are more sensitive to changes in the user-defined parameter  $\lambda$ —indeed, the errors are  
 397 similar up to  $\lambda = 0.75$ , and then they change considerably for  $\lambda = 1$ . The correlation  
 398 errors in Figure 8 change more smoothly and hence are not so sensitive to small changes

in  $\lambda$ . Such behavior is also illustrated in Figures 7a and 7b, where we see a smoother curve for the case of the mean error metric. These properties, if desired, would favor the use of the mean error metric over the maximum one.

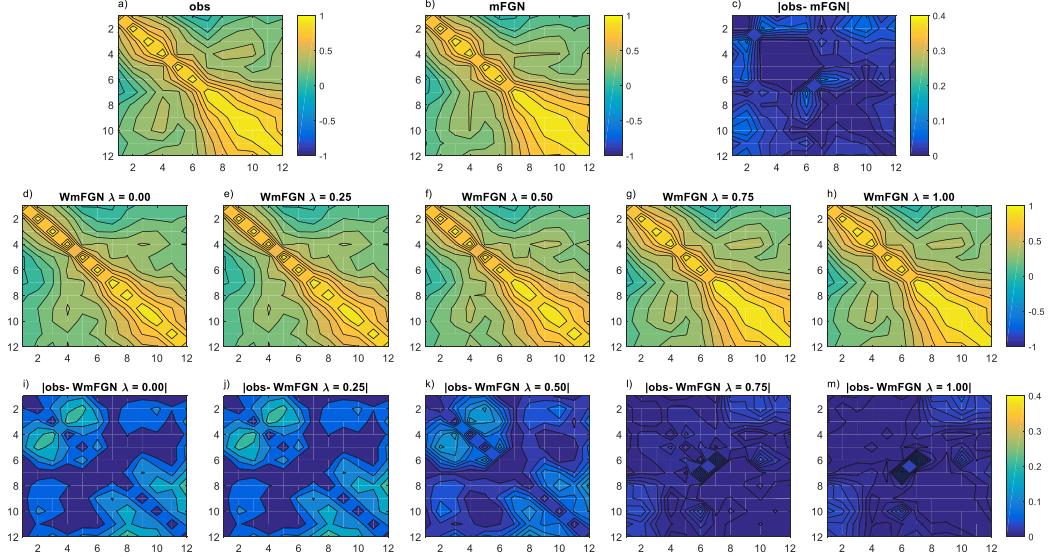


**Figure 8.** Pairwise temporal correlations of the 12 months of the year (i.e., the first month of the hydrological year is April), for the Ralco river, for different time series: a) observed, b) mFGN, c) absolute difference between observed and mFGN, d-h) WmFGN with different  $\lambda$  values, subjected to objective function 1, and i-m) absolute difference between the observed and WmFGN with different  $\lambda$  values.

## 402 5 Conclusions

403 Hydrology has used for several years the synthetic simulation of hydroclimatic variables  
 404 in different problems. Several reasons make it attractive to extrapolate historical  
 405 records, or to have the capability of analyzing the behaviour of infrastructure under con-  
 406 ditions different from the historical ones. When evaluating the design of new water in-  
 407 frastructure such as reservoirs or water facilities, stochastic methods have been used. These  
 408 tools have also shown to be useful in the evaluation of the operation of current infras-  
 409 tructure. In addition, due to challenges as climate variability and change, it does not suf-  
 410 fice to evaluate new and existing infrastructure under historical conditions. For this rea-  
 411 son, the synthetic simulation of streamflows that are not only consistent with historic

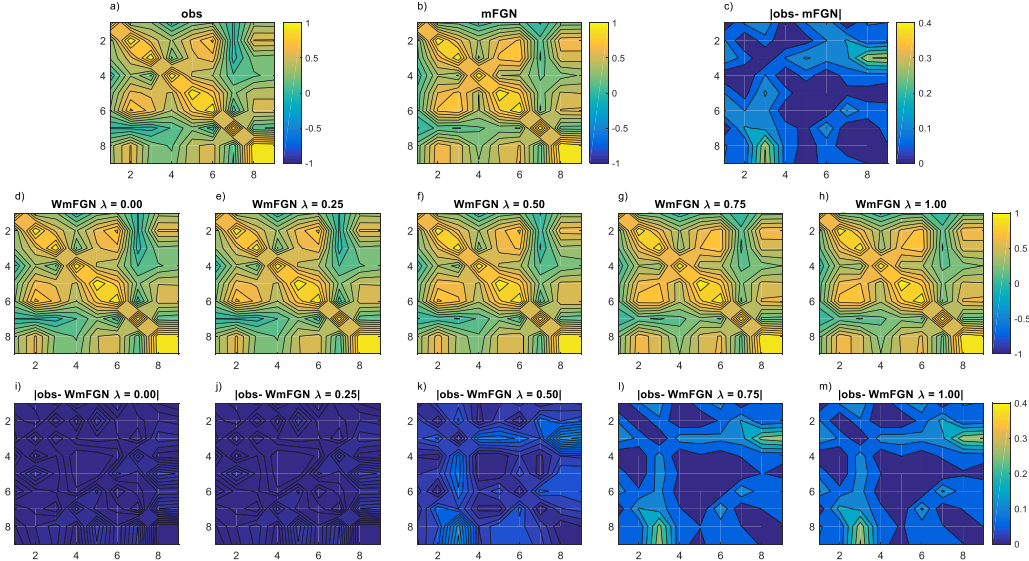


**Figure 9.** Pairwise spatial correlations of the nine river sites (i.e., the sites use the numbering from Table 1), for the month of November, for different time series: a) observed, b) mFGN, c) absolute difference between observed and mFGN, d-h) WmFGN with different  $\lambda$  values, subjected to objective function 1, and i-m) absolute difference between the observed and WmFGN with different  $\lambda$  values.

statistical properties, but also adjustable to future conditions is necessary. The stochastic models of the family of Fractional Gaussian Noise (FGN) have great potential for this.

The FGN approaches have shown to be capable of capturing long term memory in time series. Unfortunately, the original FGN procedure is not able to simulate infinite time series; that changed when the Modified FGN (mFGN) method was developed. The mFGN procedure is capable of simulating infinite time series that recreate the seasonal or periodic correlation structure, overcoming the major limitation of FGN. Also, mFGN has shown to replicate the temporal correlations of the data. However, mFGN is not well suited to represent the spatial correlation structure required to simulate several streamflows at the same time.

In this paper we have proposed a new method, called Weighted mFGN (WmFGN), that addresses both temporal and spatial correlations *simultaneously*. Our numerical experiments for a basin in Chile demonstrate that the WmFGN procedure represents a significant improvement in preserving the spatial correlation, when compared against mFGN. Moreover, since there is a trade-off in terms of representing the spatial and temporal cor-

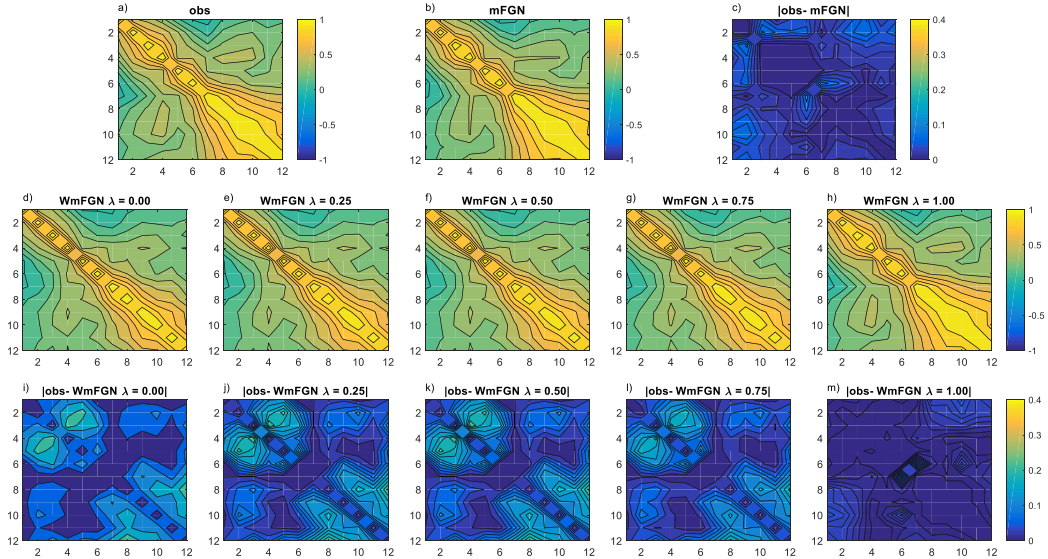


**Figure 10.** Pairwise temporal correlations of the twelve months of the year (i.e., the first month of the hydrological year is April), for the Ralco river, for different time series: a) observed, b) mFGN, c) absolute difference between observed and mFGN, d-h) WmFGN with different  $\lambda$  values, subjected to objective function 2, and i-m) absolute difference between the observed and WmFGN with different  $\lambda$  values.

relations, the method allows the user to specify the importance of one type of correlation over the other, and tailors the method for that choice by optimizing over some internal parameters. To the best of our knowledge, no other method in the literature addresses this trade-off in a systematic way.

Regardless of the trade-off, in our experiments the WmFGN procedure outperforms mFGN, even when temporal correlation is prioritized. Moreover, the higher the priority of the spatial correlation specified by the user, the higher the benefit of using WmFGN over mFGN.

As discussed earlier, the proposed approach requires the user to specify the importance of temporal correlation over the spatial one, by means of a parameter  $\lambda$  such that the weight of temporal correlation is  $\lambda$  whereas the weight of spatial correlation is  $1-\lambda$ . In the absence of a preference, the user can give equal weights to both correlations (i.e., choose  $\lambda = 0.5$ ). Note however that such a choice does not imply that the errors in both correlations (with regards to observed data) are the same; thus, another possi-

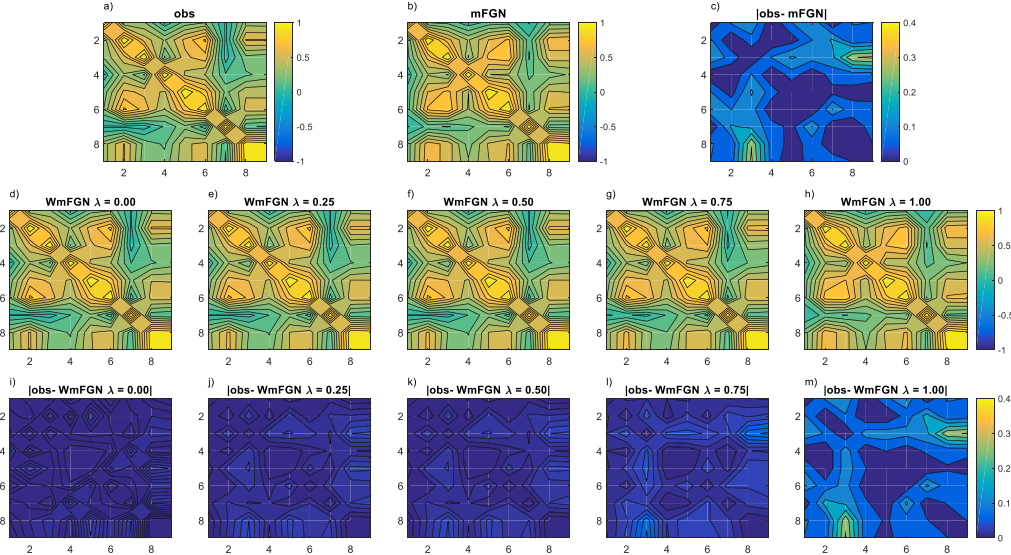


**Figure 11.** Pairwise spatial correlations of the nine river sites (i.e., the sites use the numbering from Table 1), for the month of November, for different time series: a) observed, b) mFGN, c) absolute difference between observed and mFGN, d-h) WmFGN with different  $\lambda$  values, subjected to objective function 2, and i-m) absolute difference between the observed and WmFGN with different  $\lambda$  values.

ble choice for the user is to impose that the errors in both correlations be equal, and let the method compute the corresponding value of  $\lambda$  automatically.

Finally, it is important to remember that our conclusions about the performance of WmFGN are based on the numerical experiments we have conducted. Future studies should further test the WmFGN in other basins, and also with different climates. Moreover, different error metrics can be tested; for instance, the remark in Section 2.3 suggests that other vector norms on matrices (or, more generally, other matrix norms) can be used.

#### Acknowledgments

This research was funded by grant ANILLO ACT 192094. We also acknowledge grants FONDECYT de Iniciación 11220952. We thank the National Electric Coordinator for (NEC, <https://www.coordinador.cl/reportes-y-estadisticas/#Estadisticas>) for the availability of the data.

454      **References**

- 455      Araya-Osses, D., Casanueva, A., Román-Figueroa, C., Uribe, J., & Paneque, M.  
 456      (2020). Climate change projections of temperature and precipitation in chile  
 457      based on statistical downscaling. *Climate Dynamics*, 54, 4309-4330. doi:  
 458      <https://doi.org/10.1007/s00382-020-05231-4>
- 459      Barría, P., Chadwick, C., Ocampo-Melgar, A., Galleguillos, M., Garreaud, R., Díaz-  
 460      Vasconcellos, R., . . . Poblete-Caballero, D. (2021). Water management or  
 461      megadrought: what caused the chilean aculeo lake drying? *Regional Environ-  
 462      mental Change*, 21(19). doi: <https://doi.org/10.1007/s10113-021-01750-w>
- 463      Boisier, J. P., Rondanelli, R., Garreaud, R. D., & Muñoz, F. (2016). Anthropogenic  
 464      and natural contributions to the southeast pacific precipitation decline and  
 465      recent megadrought in central chile. *Geophysical Research Letters*, 43(1),  
 466      413–421. doi: <https://doi.org/10.1002/2015GL067265>
- 467      Box, G. E., Jenkins, G. M., Reinsel, G. C., & Ljung, G. M. (2015). *Time series  
 468      analysis: forecasting and control*. John Wiley & Sons.
- 469      Brechmann, E. C., & Czado, C. (2015). Copar—multivariate time series modeling  
 470      using the copula autoregressive model. *Applied Stochastic Models in Business  
 471      and Industry*, 31(4), 495–514. doi: <https://doi.org/10.1002/asmb.2043>
- 472      CEN. (2021). *Reportes, estadísticas y plataformas de uso frecuente, developed by:  
 473      Coordinador eléctrico nacional*. Retrieved 15.11.2021, from \url{<https://www.coordinador.cl/reportes-y-estadisticas/#Estadisticas>}
- 474      Chadwick, C., Gironás, J., Gonzalez-Leiva, F., & Aedo, S. (2023). Bias-  
 475      adjustment to preserve the changes in variability: The unbiased mapping of  
 476      gcm changes to local stations. *Hydrological Science Journal*, Accepted. doi:  
 477      <https://doi.org/10.1080/02626667.2023.2201450>
- 478      Chadwick, C., Gironás, J., Vicuña, S., Meza, F., & McPhee, J. (2018). Using a  
 479      statistical preanalysis approach as an ensemble technique for the unbiased  
 480      mapping of gcm changes to local stations. *Journal of Hydrometeorology*, 19(9),  
 481      1447-1465. doi: <https://doi.org/10.1175/JHM-D-17-0198.1>
- 482      Chen, L., Singh, V. P., Guo, S., Zhou, J., & Zhang, J. (2015). Copula-based method  
 483      for multisite monthly and daily streamflow simulation. *Journal of Hydrology*,  
 484      528, 369–384. doi: <https://doi.org/10.1016/j.jhydrol.2015.05.018>
- 485      CNE. (2023). *Reporte capacidad instalada generación, marzo 2023, developed by:*

- 487        *Comisión nacional de energía.* Retrieved 15.04.2023, from \url{https://www  
 488        .cne.cl/normativas/electrica/consulta-publica/electricidad/}
- 489        de Almeida Pereira, G. A., & Veiga, Á. (2019). Periodic copula autoregressive  
 490        model designed to multivariate streamflow time series modelling. *Water  
 491        Resources Management*, 33(10), 3417–3431. doi: [https://doi.org/10.1007/  
 492        s11269-019-02308-6](https://doi.org/10.1007/s11269-019-02308-6)
- 493        Efron, B., & Tibshirani, R. J. (1994). *An introduction to the bootstrap.* CRC press.  
 494        doi: <https://doi.org/10.1201/9780429246593>
- 495        Erhardt, T. M., Czado, C., & Schepsmeier, U. (2015). R-vine models for spatial time  
 496        series with an application to daily mean temperature. *Biometrics*, 71(2), 323–  
 497        332. doi: <https://doi.org/10.1111/biom.12279>
- 498        Garreaud, R., Alvarez-Garreton, C., Brichivich, J., Boisier, J., Christie, D.,  
 499        Galleguillos, M., ... Zambrano-Bigiarini, M. (2021). The 2010-2015  
 500        megadrought in central chile: impacts on regional hydroclimate and veg-  
 501        etation. *Hydrological and Earth System Sciences*, 21, 6307-6327. doi:  
 502        <https://doi.org/10.5194/hess-21-6307-2017>
- 503        Garreaud, R., Boisier, J., Rondanelli, R., Montecinos, A., Sepúlveda, H. H., &  
 504        Veloso-Aguila, D. (2020). The central chile mega drought (2010–2018): a  
 505        climate dynamics perspective. *International Journal of Climatology*, 40(1),  
 506        421–439. doi: <https://doi.org/10.1002/joc.6219>
- 507        Gironás, J., Bunster, T., Chadwick, C., & Fernández, B. (2021). *Floods. in:*  
 508        *Fernández, b., gironás, j. (eds) water resources of chile. world water resources,*  
 509        vol 8. Springer.
- 510        Grantham, T., Figueroa, R., & Prat, N. (2013). Water management in mediter-  
 511        ranean river basins: a comparison of management frameworks, physical  
 512        impacts, and ecological responses. *Hydrobiologia*, 719, 451-482. doi:  
 513        <https://doi.org/10.1007/s10750-012-1289-4>
- 514        Hao, Z., & Singh, V. P. (2013). Modeling multisite streamflow dependence with  
 515        maximum entropy copula. *Water Resources Research*, 49(10), 7139–7143. doi:  
 516        <https://doi.org/10.1002/wrcr.20523>
- 517        Hashimoto, T., Stedinger, J., & Loucks, D. (1982). Reliability, resiliency, and  
 518        vulnerability criteria for water resource system performance evaluation.  
 519        *Water resources research*, 18(1), 14-20. doi: <https://doi.org/10.1029/>

- 520 WR018i001p00014
- 521 Herman, J. D., Zeff, H. B., Lamontagne, J. R., Reed, P. M., & Characklis, G. W.  
 522 (2016). Synthetic drought scenario generation to support bottom-up wa-  
 523 ter supply vulnerability assessments. *Journal of Water Resources Plan-  
 ning and Management*, 142(11), 04016050. doi: [https://doi.org/10.1061/\(ASCE\)WR.1943-5452.0000701](https://doi.org/10.1061/(ASCE)WR.1943-5452.0000701)
- 524 Horn, R. A., & Johnson, C. R. (2012). *Matrix analysis*, 2nd ed. Cambridge Univer-  
 525 sity Press.
- 526 IPCC. (2021). *Summary for Policymakers. In: Climate Change 2021: The Physical  
 527 Science Basis. Contribution of Working Group I to the Sixth Assessment Report of the Intergovernmental Panel on Climate Change [MassonDelmotte, V.,  
 528 P. Zhai, A. Pirani, S. L. Connors, C. Péan, S. Berger, N. Caud, Y. Chen, L.  
 529 Goldfarb, M. I. Gomis, M. Huang, K. Leitzell, E. Lonnoy, J. B. R. Matthews,  
 530 T. K. Maycock, T. Waterfield, O. Yelekçi, R. Yu and B. Zhou (eds.)] (Tech.  
 531 Rep.). Cambridge University Press. In Press.*
- 532 Jettmar, R., & Young, G. (1975). Hydrologic estimation and economic regret.  
 533 *Water Resources Research*, 11(5), 648–656. doi: <https://doi.org/10.1029/WR011i005p00648>
- 534 Kirsch, B. R., Characklis, G. W., & Zeff, H. B. (2013). Evaluating the impact  
 535 of alternative hydro-climate scenarios on transfer agreements: Practical im-  
 536 provement for generating synthetic streamflows. *Journal of Water Resources  
 537 Planning and Management*, 139(4), 396–406. doi: [https://doi.org/10.1061/\(ASCE\)WR.1943-5452.0000287](https://doi.org/10.1061/(ASCE)WR.1943-5452.0000287)
- 538 Koutsoyiannis, D. (2002). The hurst phenomenon and fractional gaussian noise  
 539 made easy. *Hydrological Sciences Journal*, 47(4), 573–595. doi: <https://doi.org/10.1080/02626660209492961>
- 540 Lall, U., & Sharma, A. (1996). A nearest neighbor bootstrap for resampling hydro-  
 541 logic time series. *Water resources research*, 32(3), 679–693. doi: <https://doi.org/10.1029/95WR02966>
- 542 Lee, T., & Salas, J. D. (2011). Copula-based stochastic simulation of hydrologi-  
 543 cal data applied to nile river flows. *Hydrology Research*, 42(4), 318–330. doi:  
 544 <https://doi.org/10.2166/nh.2011.085>
- 545 Mandelbrot, B. B., & Van Ness, J. W. (1968). Fractional brownian motions, frac-

- 553              tional noises and applications. *SIAM review*, 10(4), 422–437.
- 554              Mandelbrot, B. B., & Wallis, J. R. (1968). Noah, joseph, and operational hydrology.  
 555              *Water resources research*, 4(5), 909–918.
- 556              Mandelbrot, B. B., & Wallis, J. R. (1969). Computer experiments with fractional  
 557              gaussian noises: Part 1, averages and variances. *Water resources research*,  
 558              5(1), 228–241.
- 559              Matalas, N. C. (1967). Mathematical assessment of synthetic hydrology. *Wa-  
 560              ter Resources Research*, 3(4), 937–945. doi: <https://doi.org/10.1029/WR003i004p00937>
- 561              McLeod, A. I., & Hipel, K. W. (1978). Preservation of the rescaled adjusted range:  
 562              1. a reassessment of the hurst phenomenon. *Water Resources Research*, 14(3),  
 563              491–508.
- 564              Molinos-Senante, M., & Donoso, G. (2021). *Domestic uses of water. in: Fernández,  
 565              b., gironás, j. (eds) water resources of chile. world water resources, vol 8.* Cam-  
 566              bridge University Press.
- 567              Moreau, D. H., & Pyatt, E. E. (1970). Weekly and monthly flows in synthetic hy-  
 568              drology. *Water Resources Research*, 6(1), 53–61. doi: <https://doi.org/10.1029/WR006i001p00053>
- 569              Nataf, A. (1962). Determination des distribution don t les marges sont donnees.  
 570              *Comptes Rendus de l Academie des Sciences*, 225, 42–43.
- 571              Noakes, D. J., McLeod, A. I., & Hipel, K. W. (1985). Forecasting monthly riverflow  
 572              time series. *International Journal of Forecasting*, 1(2), 179–190. doi: [https://doi.org/10.1016/0169-2070\(85\)90022-6](https://doi.org/10.1016/0169-2070(85)90022-6)
- 573              Pagano, M. (1978). On periodic and multiple autoregressions. *The Annals of Statis-  
 574              tics*, 6(6), 1310 – 1317. doi: <https://doi.org/10.1214/aos/1176344376>
- 575              Parzen, E., & Pagano, M. (1979). An approach to modeling seasonally stationary  
 576              time series. *Journal of Econometrics*, 9(1-2), 137–153. doi: [https://doi.org/10.1016/0304-4076\(79\)90100-3](https://doi.org/10.1016/0304-4076(79)90100-3)
- 577              Pereira, G. A., Veiga, Á., Erhardt, T., & Czado, C. (2017). A periodic spatial vine  
 578              copula model for multi-site streamflow simulation. *Electric Power Systems Re-  
 579              search*, 152, 9–17. doi: <https://doi.org/10.1016/j.epsr.2017.06.017>
- 580              Reddy, M. J., & Ganguli, P. (2012). Bivariate flood frequency analysis of upper go-  
 581              davari river flows using archimedean copulas. *Water Resources Management*,

- 586                   26(14), 3995–4018. doi: <https://doi.org/10.1007/s11269-012-0124-z>
- 587     Salas, J. D., Boes, D. C., & Smith, R. A. (1982). Estimation of arma models with  
588                   seasonal parameters. *Water Resources Research*, 18(4), 1006–1010. doi:  
589                   <https://doi.org/10.1029/WR018i004p01006>
- 590     Srinivas, V., & Srinivasan, K. (2005). Hybrid moving block bootstrap for stochastic  
591                   simulation of multi-site multi-season streamflows. *Journal of Hydrology*, 302(1–  
592                   4), 307–330. doi: <https://doi.org/10.1016/j.jhydrol.2004.07.011>
- 593     Thomas Harold, A. (1962). Mathematical synthesis of streamflow sequences for the  
594                   analysis of river basin by simulation. *Design of water resources-systems*, 459–  
595                   493. doi: <https://doi.org/10.4159/harvard.9780674421042.c15>
- 596     Tsoukalas, I., Efstratiadis, A., & Makropoulos, C. (2018a). Stochastic periodic  
597                   autoregressive to anything (sparta): Modeling and simulation of cyclosta-  
598                   tionary processes with arbitrary marginal distributions. *Water Resources  
599                   Research*, 54(1), 161–185. doi: <https://doi-org.ezproxy.cul.columbia.edu/10.1002/2017WR021394>
- 600     Tsoukalas, I., Makropoulos, C., & Koutsoyiannis, D. (2018b). Simulation  
601                   of stochastic processes exhibiting any-range dependence and arbitrary  
602                   marginal distributions. *Water Resources Research*, 54(11), 9484–9513. doi:  
603                   <https://doi-org.ezproxy.cul.columbia.edu/10.1029/2017WR022462>
- 604     Vogel, R. M., & Shallcross, A. L. (1996). The moving blocks bootstrap versus para-  
605                   metric time series models. *Water resources research*, 32(6), 1875–1882. doi:  
606                   <https://doi.org/10.1029/96WR00928>
- 607     Xu, P., Wang, D., Wang, Y., & Singh, V. P. (2022). A stepwise and dynamic c-vine  
608                   copula-based approach for nonstationary monthly streamflow forecasts. *Jour-  
609                   nal of Hydrologic Engineering*, 27(1), 04021043. doi: [https://doi.org/10.1061/\(ASCE\)HE.1943-5584.0002145](https://doi.org/10.1061/(ASCE)HE.1943-5584.0002145)
- 610     Young, G., & Jettmar, R. (1976). Modeling monthly hydrologic persistence.  
611                   *Water Resources Research*, 12(5), 829–835. doi: <https://doi.org/10.1029/WR012i005p00829>

**Figure 1.**

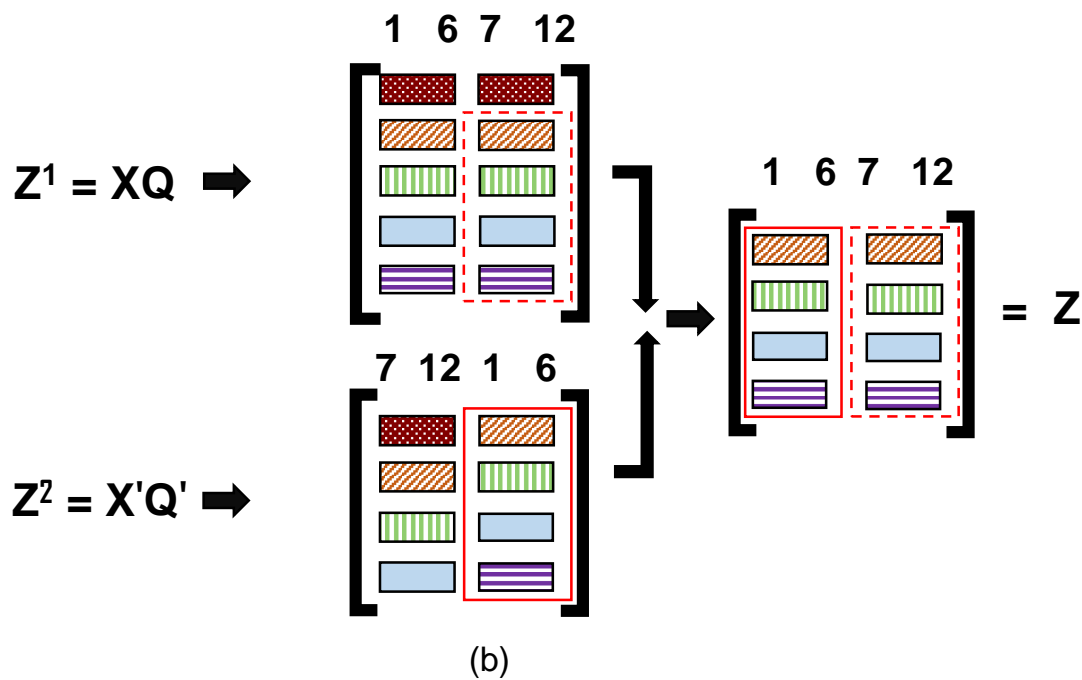
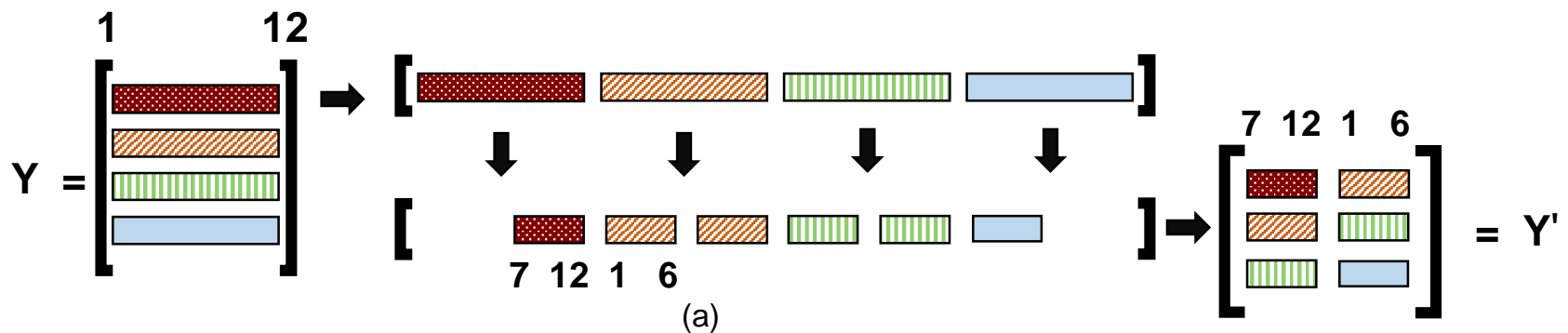


**Figure 2.**

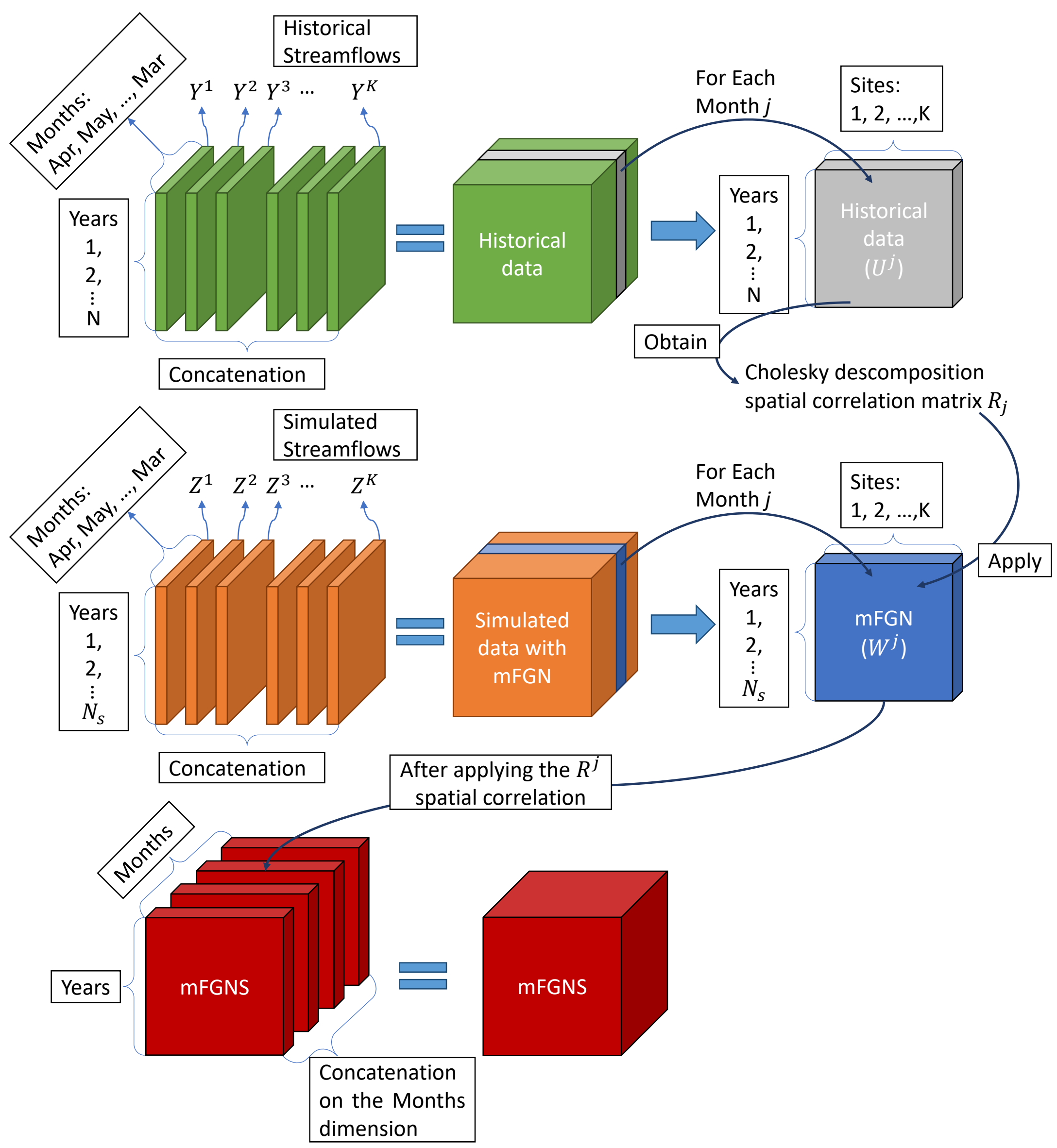


**Figure 3.**

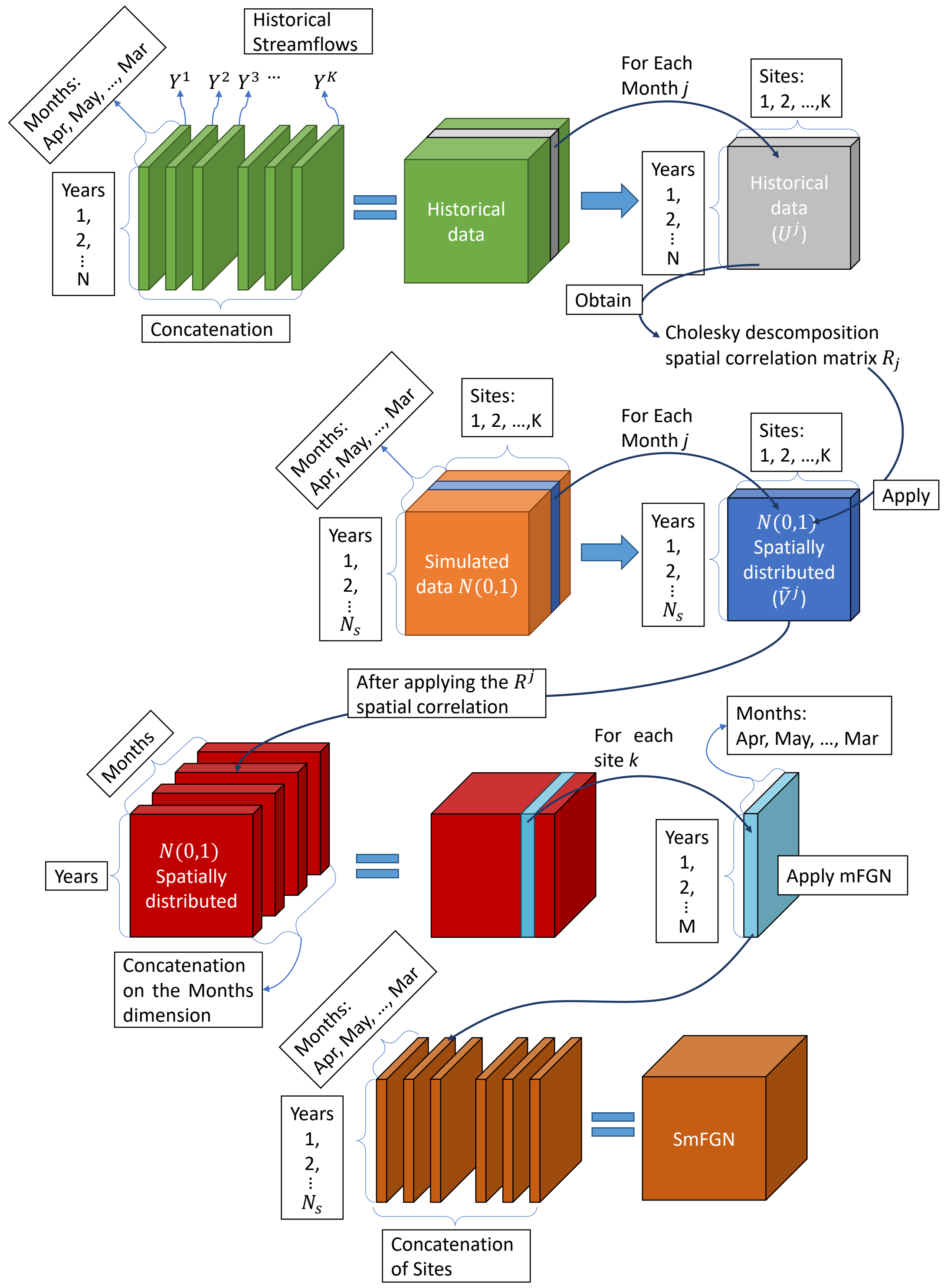


**Figure 4.**

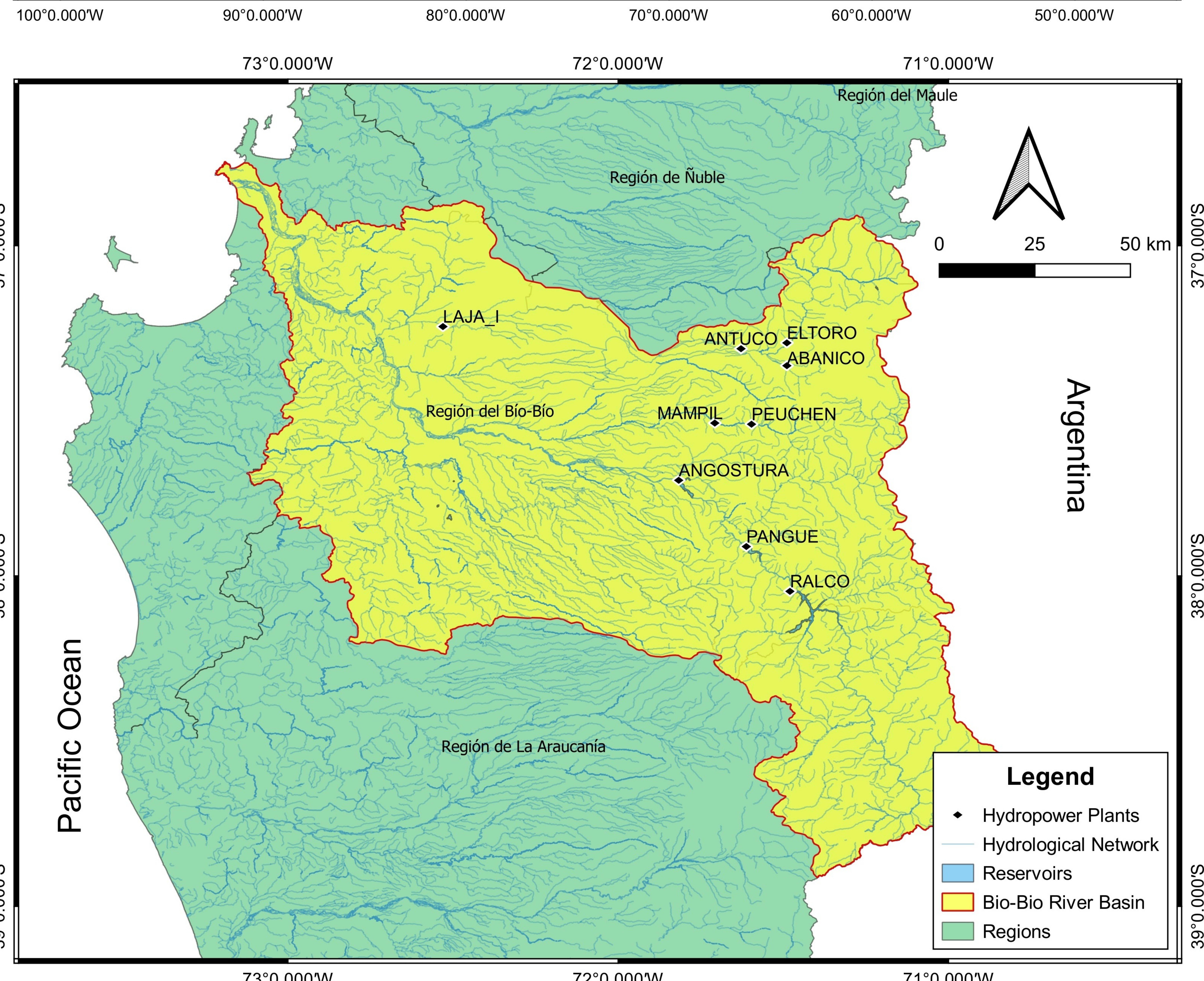
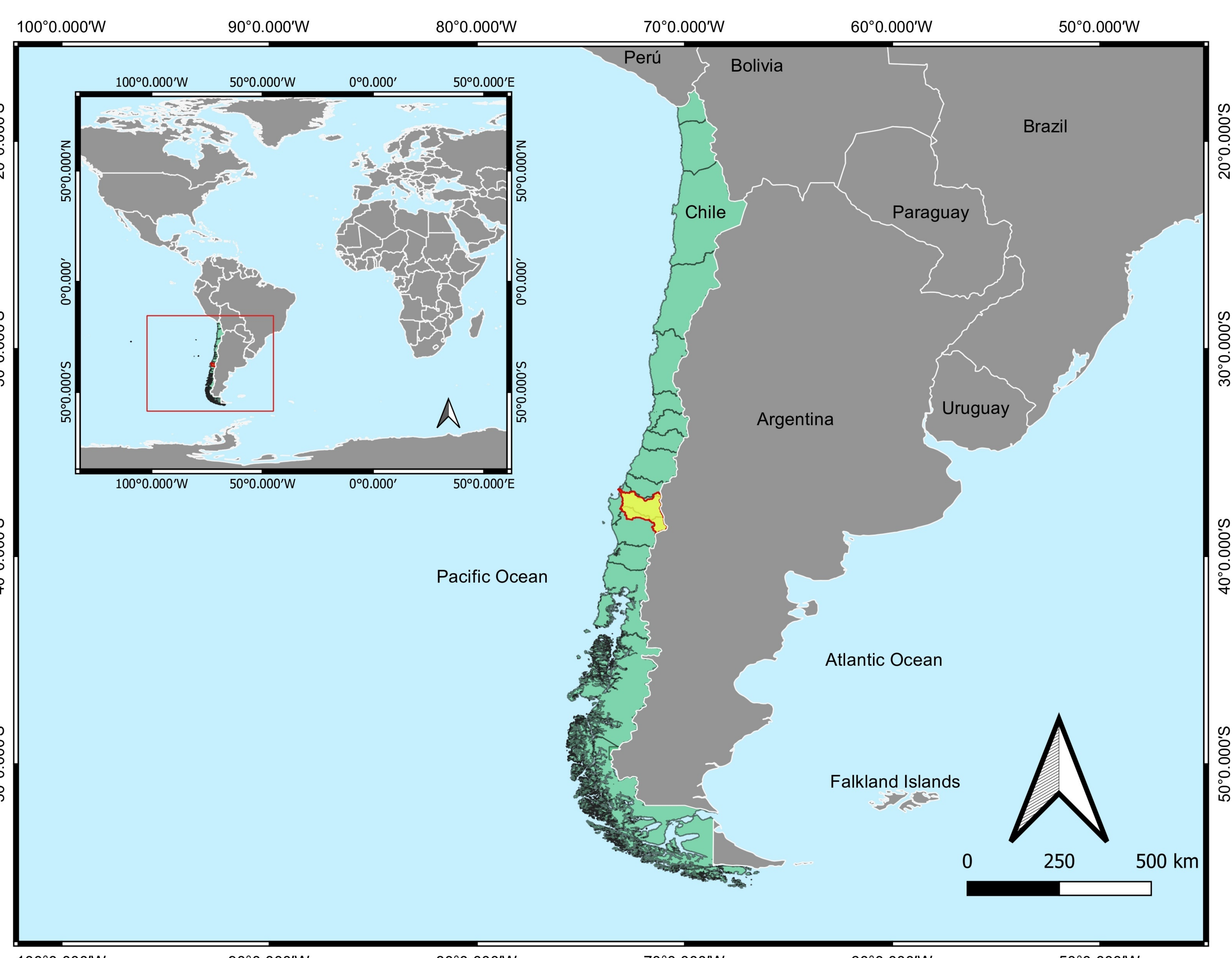


**Figure 5.**

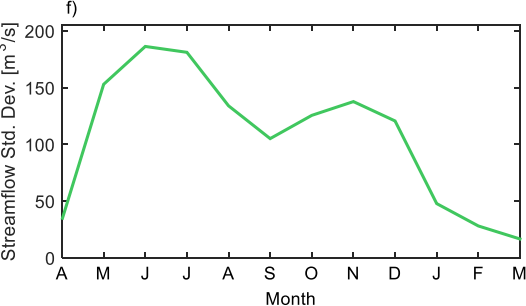
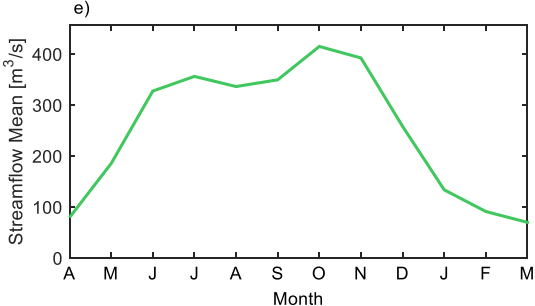
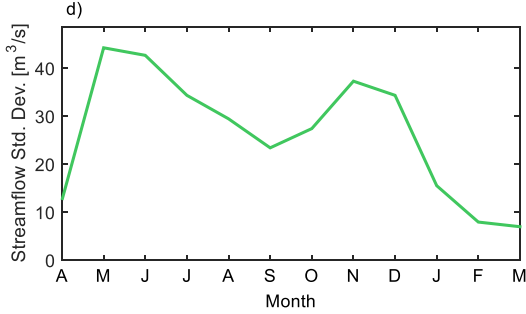
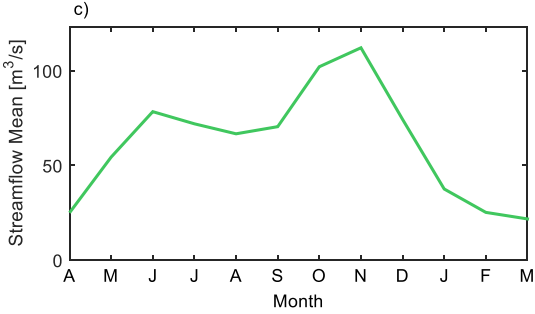
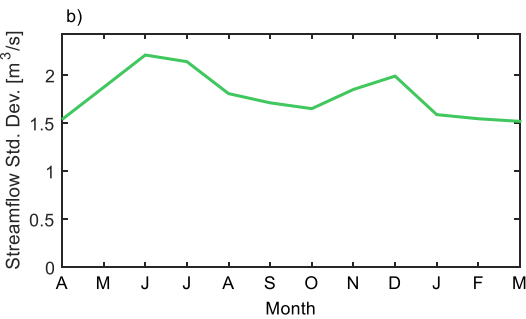
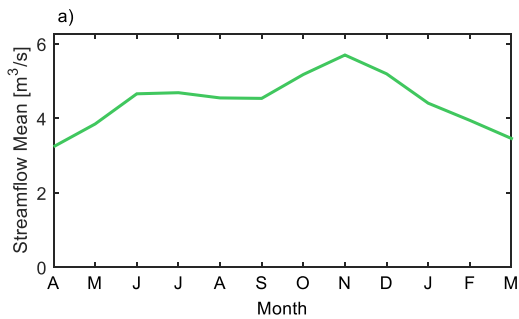


**Figure 6.**

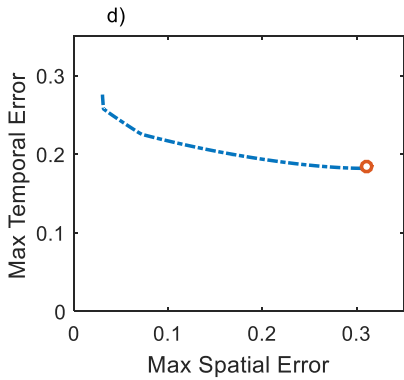
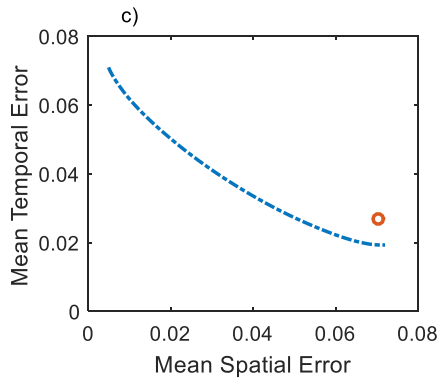
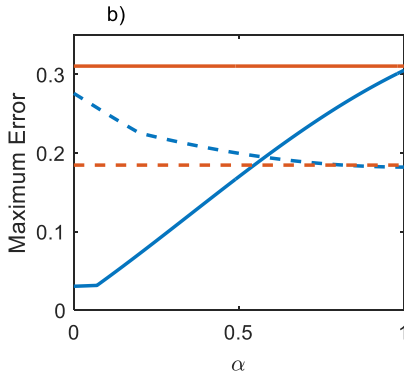
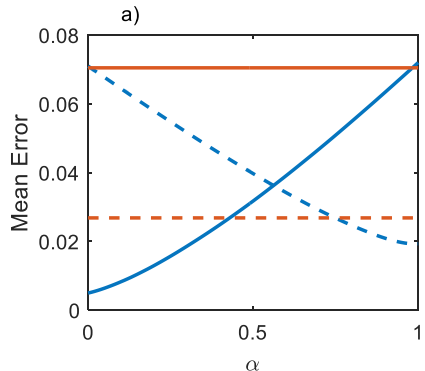


**Figure 7.**

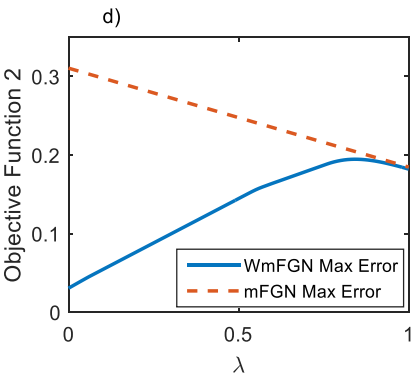
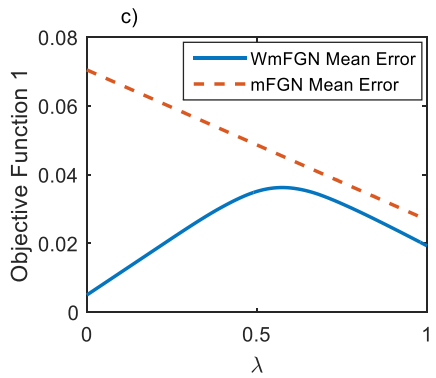
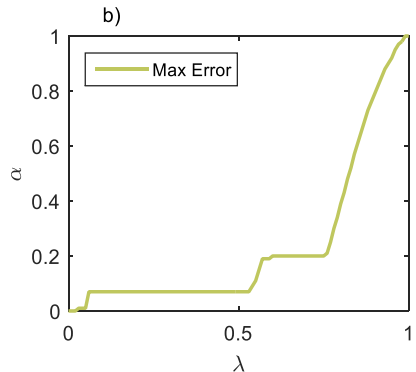
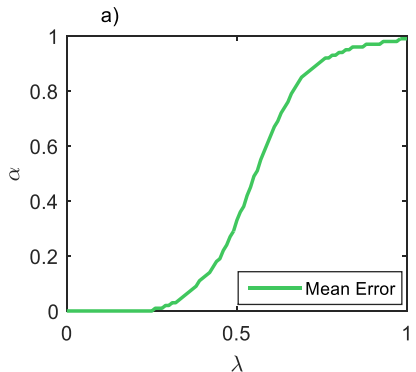


**Figure 8.**

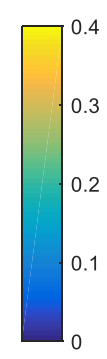
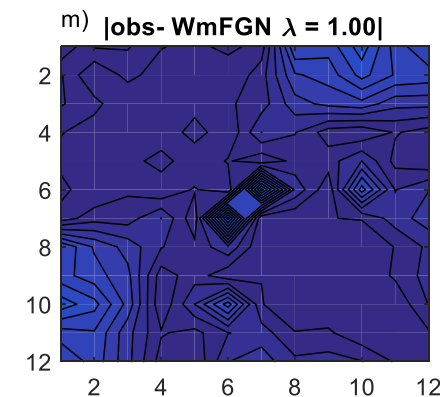
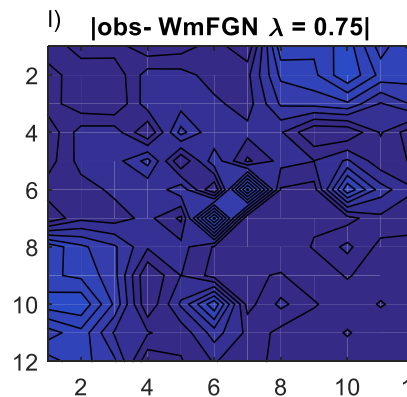
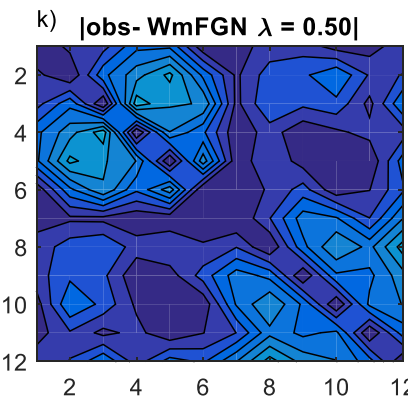
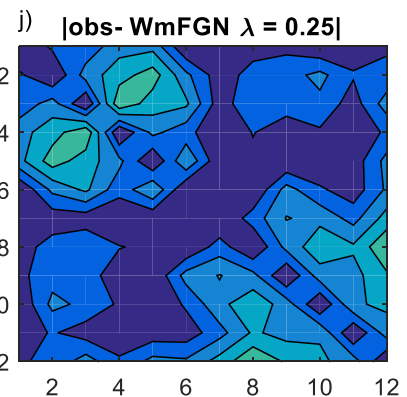
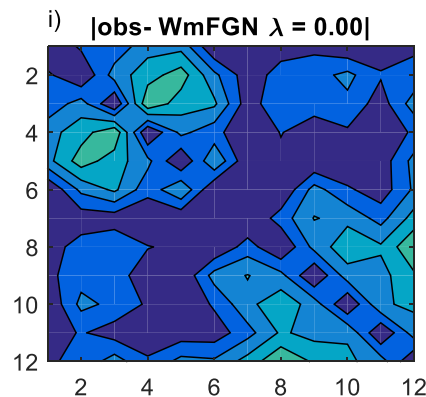
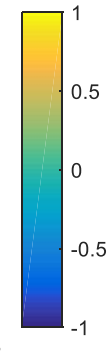
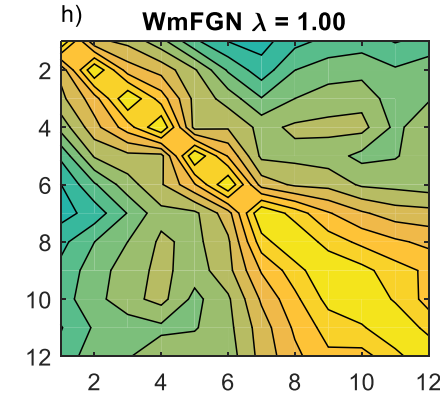
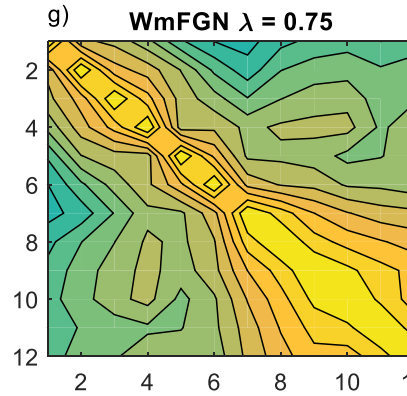
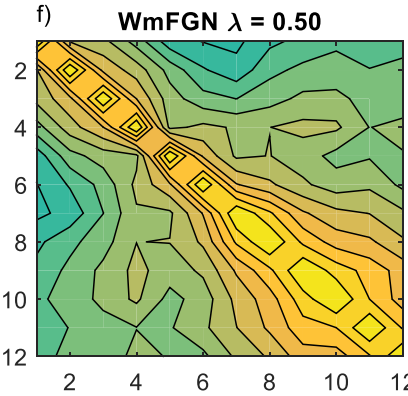
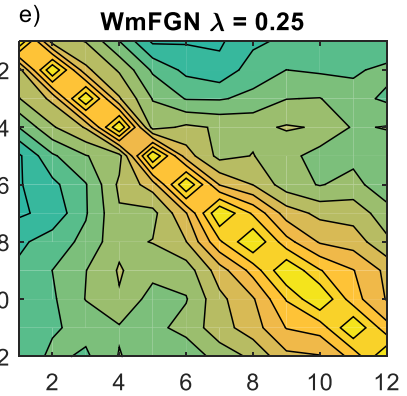
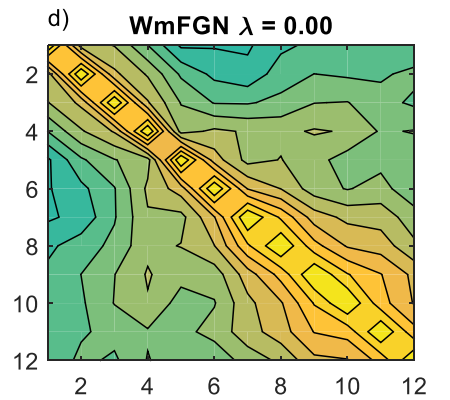
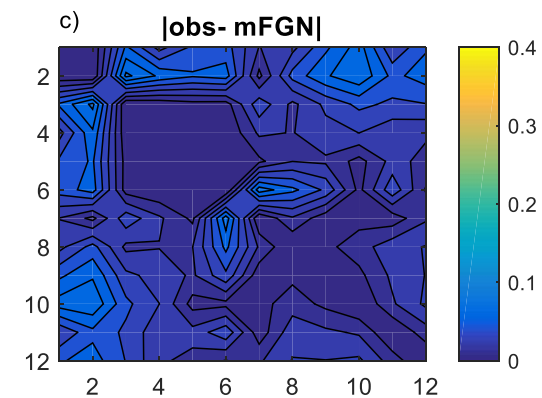
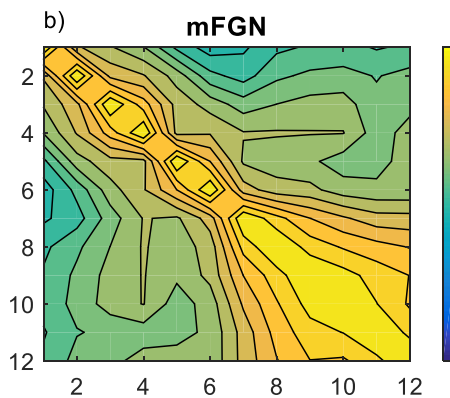
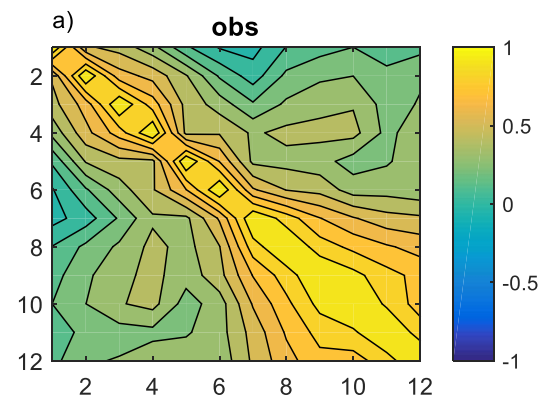


**Figure 9.**

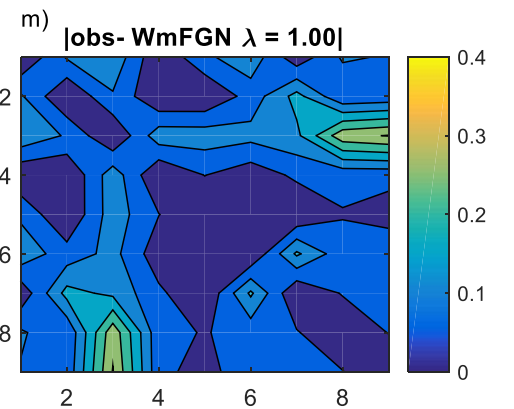
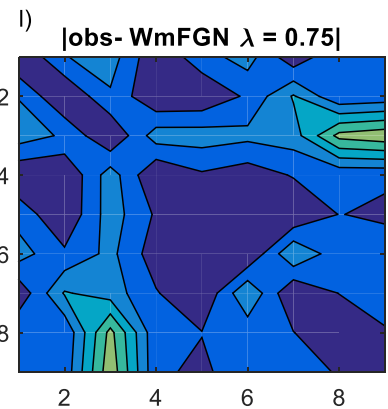
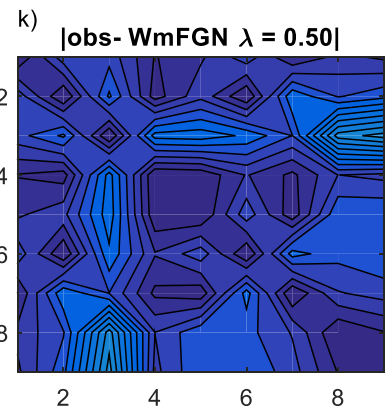
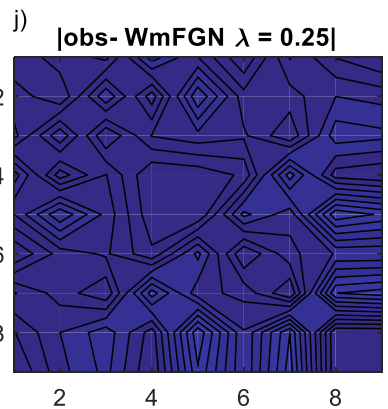
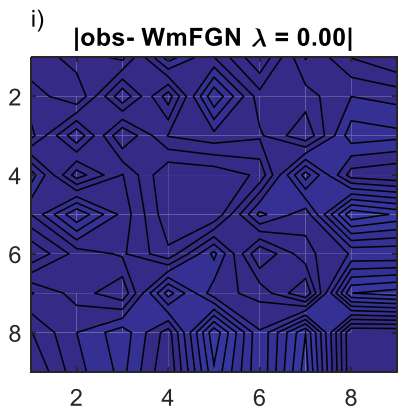
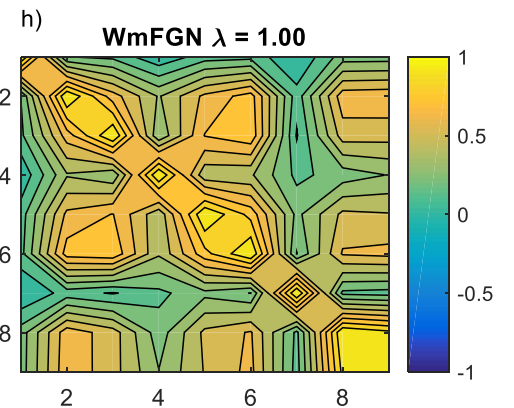
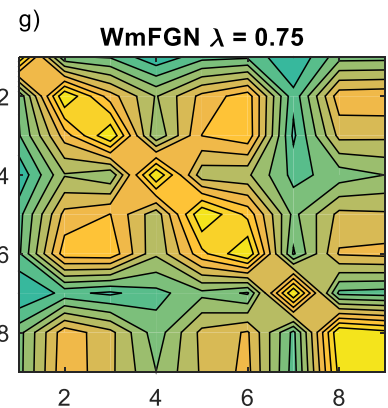
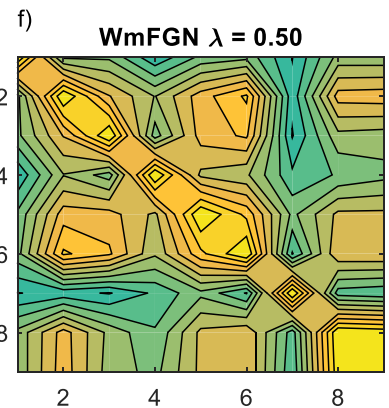
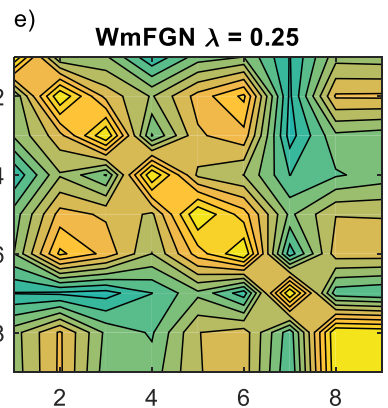
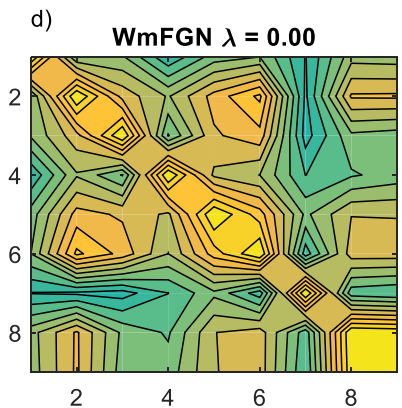
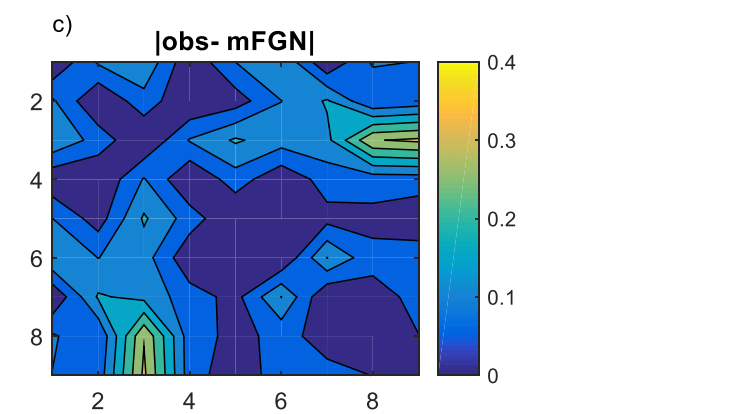
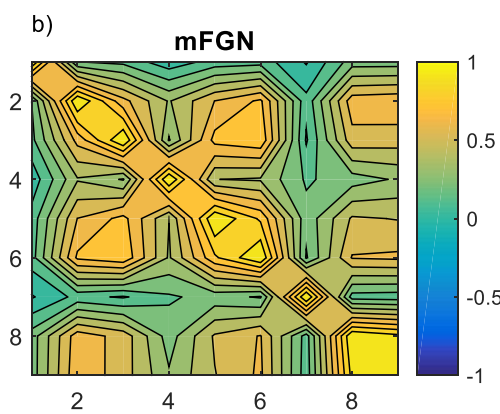
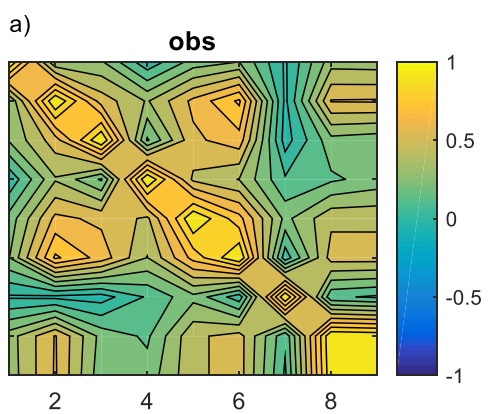


**Figure 10.**

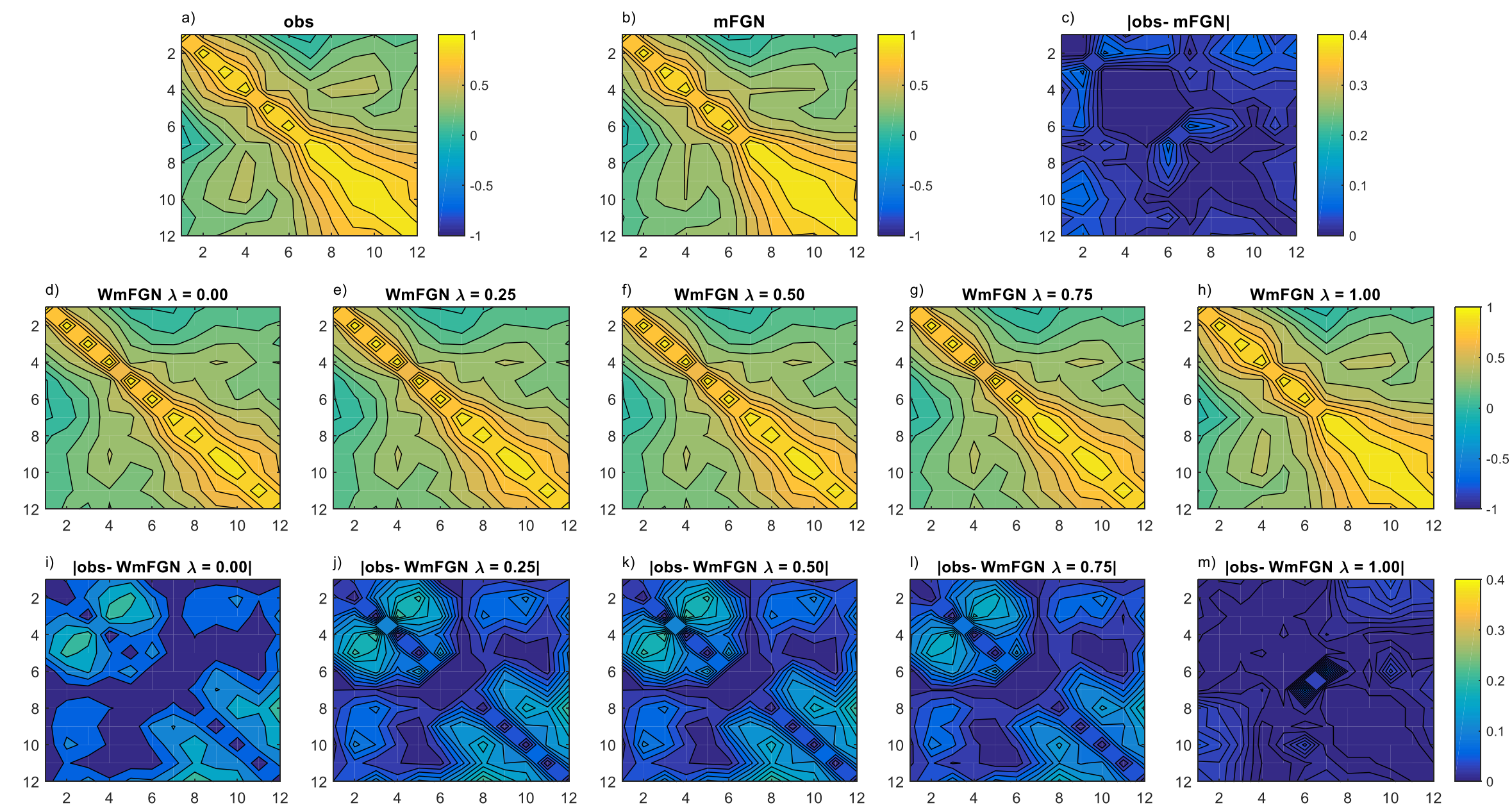


**Figure 11.**

